The Journal of Immunology

Distinct Roles for CCR4 and CXCR3 in the Recruitment and Positioning of Regulatory T Cells in the Inflamed Human Liver

This information is current as of February 24, 2022.

Ye H. Oo, Chris J. Weston, Patricia F. Lalor, Stuart M. Curbishley, David R. Withers, Gary M. Reynolds, Shishir Shetty, Jehan Harki, Jean C. Shaw, Bertus Eksteen, Stefan G. Hubscher, Lucy S. K. Walker and David H. Adams

J Immunol 2010; 184:2886-2898; Prepublished online 17 February 2010;
doi: 10.4049/jimmunol.0901216
http://www.jimmunol.org/content/184/6/2886

References This article **cites 57 articles**, 28 of which you can access for free at:
http://www.jimmunol.org/content/184/6/2886.full#ref-list-1

Why *The JI*? Submit online.

- **Rapid Reviews! 30 days*** from submission to initial decision
- **No Triage!** Every submission reviewed by practicing scientists
- **Fast Publication!** 4 weeks from acceptance to publication

**average*

Subscription Information about subscribing to *The Journal of Immunology* is online at:
http://jimmunol.org/subscription

Permissions Submit copyright permission requests at:
http://www.aai.org/About/Publications/JI/copyright.html

Email Alerts Receive free email-alerts when new articles cite this article. Sign up at:
http://jimmunol.org/alerts

The Journal of Immunology is published twice each month by
The American Association of Immunologists, Inc.,
1451 Rockville Pike, Suite 650, Rockville, MD 20852
Copyright © 2010 by The American Association of Immunologists, Inc. All rights reserved.
Print ISSN: 0022-1767 Online ISSN: 1550-6606.

Downloaded from http://www.jimmunol.org/ by guest on February 24, 2022

Distinct Roles for CCR4 and CXCR3 in the Recruitment and Positioning of Regulatory T Cells in the Inflamed Human Liver

Ye H. Oo,*,† Chris J. Weston,* Patricia F. Lalor,* Stuart M. Curbishley,* David R. Withers,‡ Gary M. Reynolds,* Shishir Shetty,* Jehan Harki,* Jean C. Shaw,* Bertus Eksteen,*,† Stefan G. Hubscher,* Lucy S. K. Walker,‡ and David H. Adams*,†

Regulatory T cells (T_{regs}) are found at sites of chronic inflammation where they mediate bystander and Ag-specific suppression of local immune responses. However, little is known about the molecular control of T_{reg} recruitment into inflamed human tissues. We report that up to 18% of T cells in areas of inflammation in human liver disease are forkhead family transcriptional regulator box P3 (FoxP3)$^+$ T_{regs}. We isolated $CD4^+CD25^+CD127^{low}FoxP3^+$ T_{regs} from chronically inflamed human liver removed at transplantation; compared with blood-derived T_{regs}, liver-derived T_{regs} express high levels of the chemokine receptors CXCR3 and CCR4. In flow-based adhesion assays using human hepatic sinusoidal endothelium, T_{regs} used CXCR3 and α4β1 to bind and transmigrate, whereas CCR4 played no role. The CCR4 ligands CCL17 and CCL22 were absent from healthy liver, but they were detected in chronically inflamed liver where their expression was restricted to dendritic cells (DCs) within inflammatory infiltrates. These DCs were closely associated with CD8 T cells and $CCR4^+$ T_{regs} in the parenchyma and septal areas. Ex vivo, liver-derived T_{regs} migrated to CCR4 ligands secreted by intrahepatic DCs. We propose that CXCR3 mediates the recruitment of T_{regs} via hepatic sinusoidal endothelium and that CCR4 ligands secreted by DCs recruit T_{regs} to sites of inflammation in patients with chronic hepatitis. Thus, different chemokine receptors play distinct roles in the recruitment and positioning of T_{regs} at sites of hepatitis in chronic liver disease. ***The Journal of Immunology*, 2010, 184: 2886–2898.**

Immune homeostasis is dependent on the ability of the immune system to respond to pathogens while suppressing responses to self-Ags and harmless environmental Ags. The maintenance of tolerance to self-Ags involves central and peripheral mechanisms. T regulatory cells (T_{regs}) are a subset of T lymphocytes that play a crucial role in maintaining peripheral tolerance by suppressing self-reactive T cells and preventing collateral autoimmune damage as a consequence of immune responses to infections (1). T_{regs} are also implicated in the tolerogenic properties of the liver and help to suppress responses to harmless food Ags and bacterial components to which the liver is constantly exposed via the portal vein (2).

T_{regs} have been implicated in several inflammatory liver diseases. It has been suggested that their frequency is increased in the liver in chronic viral hepatitis, in which a failed immune response leads to viral persistence, and in hepatocellular carcinoma, in which protective antitumor immune responses may be suppressed (3, 4). In contrast, there is evidence for reduced T_{reg} frequency and defective function in autoimmune liver disease (5, 6).

Naturally occurring T_{regs} are thymus-derived cells that are present from birth. They are defined by the expression of CD4, CD25, and the forkhead family transcriptional regulator box P3 (FoxP3), which is required for their development and function (7), and low expression of the IL-7 receptor (CD127) (8–10). T_{regs} suppress effector cell proliferation and cytokine production in vitro in a cell contact-dependent manner and protect against autoimmunity following adoptive transfer in vivo (11). In the healthy organism, T_{regs} suppress effector T cell activation in secondary lymphoid tissues to maintain steady-state self-tolerance. However, in chronic inflammatory states and autoimmune disease, T_{regs} are detected at sites of inflammation where they suppress immune responses locally (12–17). Thus, when steady-state self-tolerance is breached as a consequence of infection or chronic inflammation, T_{regs} become further activated to allow their migration into peripheral tissue where they limit local bystander and collateral damage. The ability to enter peripheral tissues, such as the liver, requires the downregulation of chemokine receptors and adhesion molecules, such as CCR7 and L-selectin, which promotes entry to secondary lymphoid tissues and the expression of receptors required for recruitment into sites of inflammation. Little is known about the receptors involved in the recruitment and positioning of T_{regs} in chronically inflamed human tissues. In the current study, we report that chronic inflammatory liver disease is associated with a high frequency of liver-infiltrating $CD4^+CD25^+CD127^{low}FoxP3^+$ T_{regs} that are detected in close association with intrahepatic dendritic cells (DCs) at sites of inflammation. We show that liver-

*Centre for Liver Research, Institute of Biomedical Research and ‡Medical Research Council Centre for Immune Regulation, The University of Birmingham Medical School; and †The National Institute for Health Research Biomedical Research Unit, Queen Elizabeth Hospital, Edgbaston, Birmingham, United Kingdom

Received for publication April 15, 2009. Accepted for publication December 29, 2009.

This work was supported by grants from the Medical Research Council (fellowships to Y.H.O., B.E., and L.S.K.W.), Core (fellowship to S.S.), the Wellcome Trust, National Institute for Health Research, and the National Institutes of Health (5RO1AA014257).

Address correspondence and reprint requests to Dr. David H. Adams, Centre for Liver Research, Institute of Biomedical Research, The National Institute for Health Research Biomedical Research Unit, University of Birmingham, Birmingham, B15 2TT, United Kingdom. E-mail address: d.h.adams@bham.a.uk

Abbreviations used in this paper: AIH, autoimmune hepatitis; ALD, alcoholic liver disease; DC, dendritic cell; FoxP3, forkhead family transcriptional regulator box P3; HCV, chronic hepatitis C virus; HSEC, hepatic sinusoidal endothelial cell; LIDC, liver-infiltrating dendritic cell; LIL, liver-infiltrating lymphocyte; LIT_{reg}, liver-infiltrating regulatory T cell; MoDC, monocyte-derived dendritic cell; NANB, non-A non-B seronegative hepatitis; NASH, nonalcoholic steatohepatitis; NL, normal liver (donor, control); P, parenchyma; PBC, primary biliary cirrhosis; PBT_{reg}, peripheral blood regulatory T cell; phosphoSTAT5, phosphorylated STAT5; PSC, primary sclerosing cholangitis; PT, portal tract; PTx, pertussis toxin; T_{reg}, regulatory T cell; TRITC, tetramethylrhodamine isothiocyanate.

Copyright © 2010 by The American Association of Immunologists, Inc. 0022-1767/10/$16.00

www.jimmunol.org/cgi/doi/10.4049/jimmunol.0901216

Downloaded from http://www.jimmunol.org/ by guest on February 24, 2022

infiltrating T_{regs} (LIT_{regs}) use CXCR3 to undergo transendothelial migration across hepatic sinusoidal endothelium and use CCR4 to respond to CCL17 and CCL22 secreted by intrahepatic DCs. Thus, different chemokine receptors play distinct roles in the recruitment and positioning of T_{regs} at sites of hepatitis in chronic liver disease.

Materials and Methods

Tissues and blood

Venous blood was obtained from patients undergoing liver transplantation before induction of anesthesia and before any blood transfusion. Subsequently, explanted diseased liver was obtained from the same patients to allow the isolation of matched blood- and liver-derived cells. Nondiseased liver tissue was obtained from donor liver tissue surplus to clinical requirements or from uninvolved liver tissue removed at the time of resection for colorectal hepatic metastases. All samples were collected with appropriate patient consent and local research ethics committee approval.

Abs and reagents

The following primary Abs were used for immunohistochemistry, immunofluorescence, and confocal microscopy: mouse anti-human CCL22 mAb (MAB 336, R&D Systems, Minneapolis, MN), goat anti-human CCL17 mAb (AF 364, R&D Systems), mouse anti-human FoxP3 (Abcam, 236A/E7, Cambridge, U.K.), rabbit anti-human polyclonal to CCL22 amino terminal end (Ab 53002-100; Abcam), rabbit anti-human monoclonal to CD11c (Abcam, EP13474), rabbit monoclonal to phosphorylated STAT5 (phosphoSTAT5)(Abcam/E208), mouse anti-human CD4 IgG 2b (eBioscience, Hatfield, U.K.), anti-human CD3 IgG2a (eBioscience), and mouse anti-human CD8 IgG2a (eBioscience). Relevant secondary Abs used were anti-IgG1 FITC (Southern Biotech, Cambridge, U.K.), rabbit-anti FITC (Sigma-Aldrich, St. Louis, MO), goat-anti rabbit FITC (Southern Biotech), anti-IgG2b biotinylated (Southern Biotech), anti-IgG1 biotinylated (Southern Biotech), streptavidin 555 (Invitrogen, Paisley, U.K.), streptavidin 647 (Invitrogen), mouse anti-human IgG2a Cy-3 (Southern Biotech), and goat anti-mouse IgG1 FITC (Southern Biotech).

The following Abs were used for multicolor flow cytometry: mouse anti-human CD4 Pacific Blue (RPA-T4, BD Pharmingen, San Diego, CA), mouse anti-human CD25 PE Cy-5 (IM2646, Beckman Coulter, Fullerton, CA), mouse anti-human CD3 PE-Cy7 (UCHT-1, eBioscience), mouse anti-human CD127 Alexa-488 (Biolegend, Cambridge, U.K.; HCD127), mouse anti-human APC Cy-7 CD27 (O323, Biolegend), mouse anti-human CD39 PE (Clone eBio A1, eBioscience), mouse anti-human CD134/OX40 (555838, BD Pharmingen), rat anti-human Foxp3 PE (PCH 101, eBioscience), and CD45 RO PE Cy-5 (UCHL-1, BD Pharmingen). CCR1 mAb (53504/ FAB145P, 1/10), CCR2 mAb (48607/FAB151P), CCR3 mAb (61828/FAB155P), CCR4 mAb (205410/FAB 1567P, FAB1567F), CCR5 mAb (CTC5/FAB1802P), CCR6 mAb (53103/FAB 195P), CCR7 mAb (150503/FAB197P), CCR8 mAb (191704/FAB1429P), CCR9 mAb (112509/FAB179P), CCR10 mAb (FAB3478P), CXCR1 mAb (42705/FAB330P), CXCR2 mAb (48311/FAB331P), CXCR3 mAb (FAB160P, FAB160F), CXCR3 mAb (550967; BD), CXCR4 mAb (12G5/FAB170P), CXCR5 mAb (51505/FAB190P), and CXCR6 mAb (56811/FAB699P) were

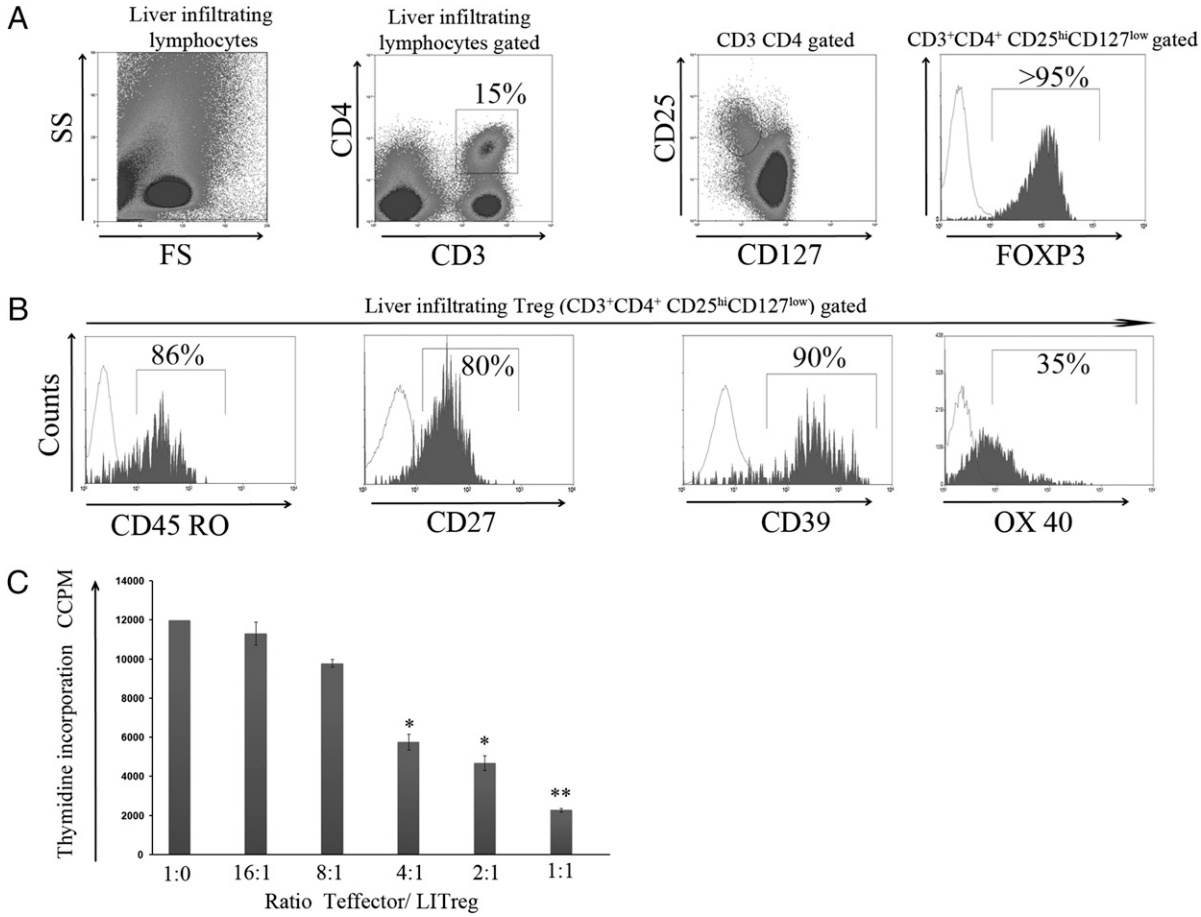

FIGURE 1. Phenotype of LIT_{regs} freshly isolated from explanted human liver without expansion in vitro. *A*, Human LILs were stained for cell surface expression of CD4, CD25, and CD127. The stained cells were fixed, permeabilized, and stained intracellularly for FoxP3. For analysis, LILs were gated on forward scatter and side scatter, and LIT_{regs} were identified by gating on $CD3^{high}CD4^{high}$ lymphocytes, followed by $CD25^{high}$ (*y*-axis) and $CD127^{low}$ (*x*-axis). The square box represents the population of LIT_{regs}. Graph shows the expression of transcription factor FoxP3, which was analyzed on LIT_{regs} ($CD3^{high}CD4^{high}CD25^{high}CD127^{low}$) by flow cytometry. *B*, Flow cytometry overlay histograms show the percentage of LIT_{regs} positive for CD45RO, CD27, CD39, or OX-40. The percentage expression of relevant markers are provided. Representative data of one of six independent experiments. *C*, The suppressive function of freshly isolated human LIT_{regs} was assessed by [^{3}H]thymidine proliferation. LIT_{regs} were isolated using the Dynal T_{reg} isolation kit from freshly isolated liver-derived lymphocytes. Suppression of proliferation was done at ratios of 1:16 to 1:1 freshly isolated LIT_{regs}/naive lymphocytes activated by allogenic liver-derived DCs. Data represent mean ± SEM of three independent experiments. $*p < 0.05$; $**p < 0.005$ by Student *t* test.

Downloaded from http://www.jimmunol.org/ by guest on February 24, 2022

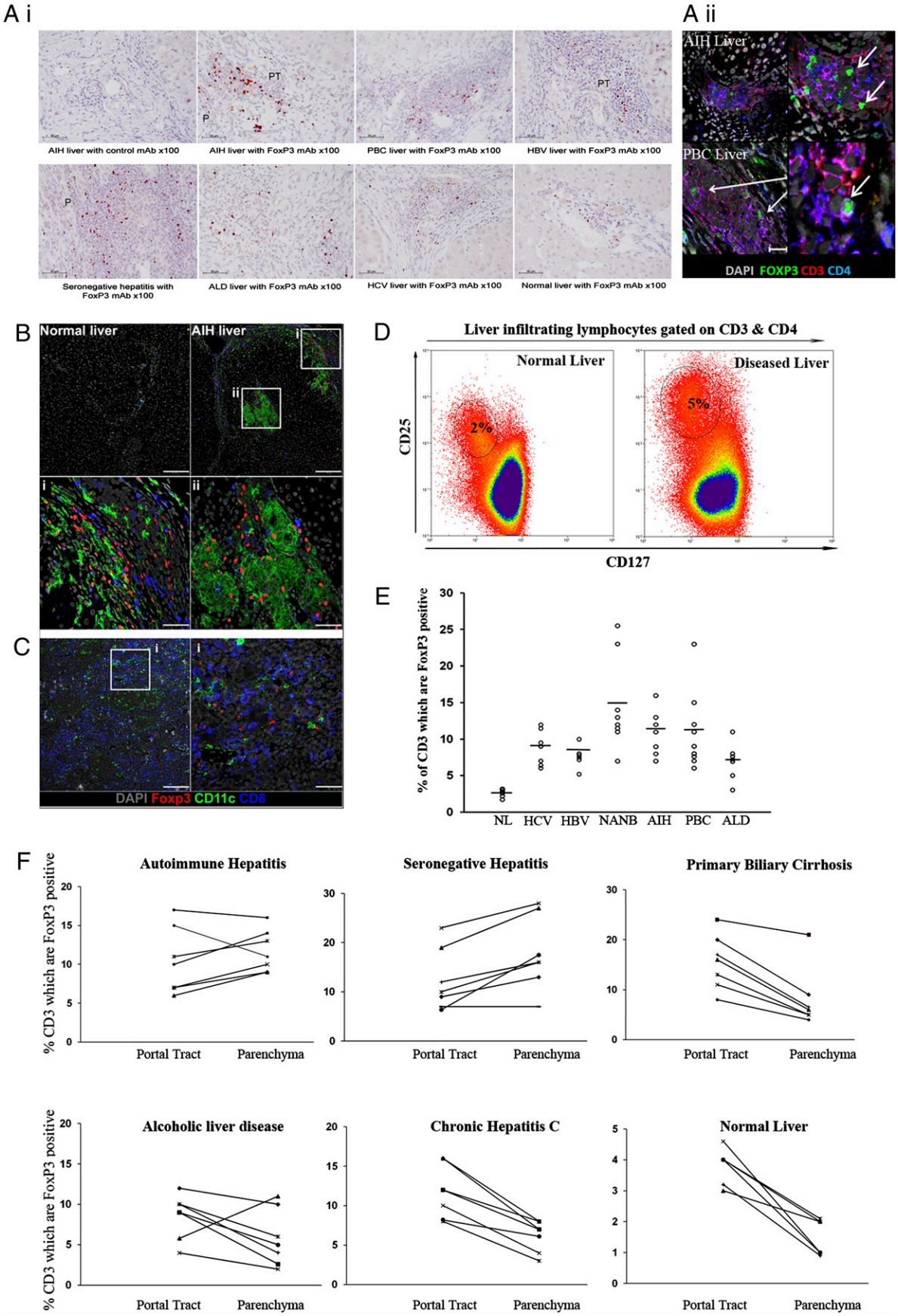

FIGURE 2. Detection of T_{regs} in different liver diseases and portal lymph node. *Ai*, Single immunohistochemical staining of formalin-fixed, paraffin-embedded liver sections revealed FoxP3$^+$ cells staining using mAb (Abcam clone 236A/E7) (detected as a brown pigment) in PT and parenchyma (P) of patients with NL and different chronic liver diseases: AIH, ALD, non-A non-B (seronegative) hepatitis, PBC, chronic hepatitis B (HBV), and chronic HCV. FoxP3$^+$ cells in liver tissue are indicated by arrows. Control sections are stained with isotype-matched IgG (original magnification ×100). *Aii*, Expression

Downloaded from http://www.jimmunol.org/ by guest on February 24, 2022

purchased from R&D Systems. For intracellular cytokine staining, FITC-conjugated mAb to IFN-γ (340449, BD Pharmingen), FITC-conjugated mAb to IFN-γ (MHCIFG05, Caltag Laboratories, Buckingham, U.K.), and FITC-conjugated mAb to TNF-α (554512, BD Pharmingen) were used.

Liver-infiltrating lymphocyte and LIT_{reg} isolation

Liver-infiltrating lymphocytes (LILs) were isolated from fresh liver tissue, as previously described (18, 19). To maximize yield and viability, LIT_{regs} were isolated immediately after explantation of livers from patients with various liver diseases, including alcoholic cirrhosis, nonalcoholic steatohepatitis, primary biliary cirrhosis (PBC), and autoimmune hepatitis (AIH). Liver tissue was diced into 5-mm^3 cubes and subjected to mechanical homogenization in a Seward stomacher 400 circulator (230 rpm for 5 min), without the use of an enzymatic-digestion step, which removes some chemokine receptors. The resulting homogenate was filtered through fine gauze, and lymphocytes were separated using Lympholyte (VH Bio, Gateshead, U.K.) density gradient centrifugation (650 × *g* for 30 min). The lymphocyte band was removed and washed, and cell viability was assessed by trypan blue exclusion. T_{regs} were purified from the total lymphocyte population by negative selection to remove $CD8^+$ cells and positive selection of $CD4^+CD25^+$ cells with a T_{reg} isolation kit (DYNAL, Invitrogen). LIT_{regs} were defined using cell surface staining as $CD3^+$, $CD4^+$, $CD25^{high}$, or $CD127^{low}$, and intracellular staining (fix & perm kit from eBioscience) was used to confirm the expression of FoxP3.

The purity of T_{regs} isolated using the $CD4^+CD25^+$ T_{reg} kit was confirmed to be >95% by flow cytometry, and T_{reg} status was confirmed by Foxp3 RT-PCR (data not shown). Following isolation, T_{regs} were cultured in RPMI 1640, 10% human serum, streptomycin (100 U/ml), penicillin (100 IU/ml), glutamine (2 mmol/l), and IL-2 (500 U/ml) in round-bottom 96-well culture plates.

PBL and peripheral blood T_{reg} isolation

Lymphocytes were isolated from peripheral venous blood by density gradient centrifugation over a Lympholyte gradient (30 min at 650 × *g*). Peripheral blood T_{regs} (PBT_{regs}) were purified, as described above, using a T_{reg} isolation kit and phenotyped using CD4, $CD25^{high}$, $CD127^{low}$, and intracellular FoxP3 expression to define T_{regs}. Purity was confirmed by flow cytometry, as described above.

Isolation and culture of liver-derived DCs and monocyte-derived DCs

Liver-infiltrating DCs (LIDCs) were isolated from diseased liver using a method established in our laboratory (20). Briefly, after isolation of lymphocytes, followed by a 13.5% OptiPrep density gradient (Axis Shield, Cambridge, U.K.), CD11c-positive magnetic selection was used to obtain highly purified DCs. Monocyte-derived DCs (MoDCs) from peripheral blood were isolated according to established methods, as previously described (21). Briefly, OptiPrep was added to buffy coats made from whole blood to increase its density to ~1.1 g/ml, overlayered by two different density solutions of OptiPrep (1.068 and 1.084 g/ml), and centrifuged at 750 × *g* for 20 min. The monocytes in the 1.068-g/ml layer were collected and cultured for 5 d in media containing RPMI 1640, 5% FCS, and 10 ng/ml IL-4 (BD Pharmingen) with 1000 U/ml recombinant human GM-CSF (Mielogen; Schering-Plough, Kenilworth, NJ), after which the immature DCs were matured with TNF-α. To obtain highly pure DCs, these cells underwent positive immunomagnetic selection with CD11c.

Isolation and culture of hepatic sinusoidal endothelial cells

Hepatic sinusoidal endothelial cells (HSECs) were isolated according to methods established in our laboratory (22). Explanted liver tissue (~30 g) was finely chopped and subjected to enzymatic digestion (1 mg/ml, collagenase type IV; Sigma-Aldrich) and density gradient centrifugation (Percoll; Amersham Biosciences, GE Healthcare, Little Chalfont, U.K.). The nonparenchymal cell band was removed and further purified by immunomagnetic selection using mAb HEA-125 (PROGEN, Heidelberg, Germany) to remove cholangiocytes. CD31 (DAKO) was used to select HSECs, which were plated in collagen-coated 25-cm^2 tissue culture flasks (Corning Glass, Londonborough, U.K.) and cultured in human endothelial basal media (Invitrogen) containing 10% human serum (H&D Supplies, Bucks, U.K.), penicillin, streptomycin (100 IU/ml), glutamine (2 mmol/l), hepatocyte growth factor (10 ng/ml, PeproTech, Peterborough, U.K.), and vascular endothelial growth factor (10 ng/ml, PeproTech). Cells were cultured to confluence and were used between passages two and four in all experiments.

Immunohistochemistry

Formalin-fixed paraffin-embedded liver specimens from seven cases each of normal liver (NL), AIH, alcoholic liver disease (ALD), PBC, fulminant seronegative hepatitis or non-A non-B hepatitis, chronic hepatitis B virus, and chronic hepatitis C virus (HCV); five portal draining lymph nodes were examined. The tonsil/lymph node tissues were used as positive control, and negative controls were used for each staining as well. The liver tissue sections were dewaxed in xylene for 10 min and incubated through different strengths of alcohol. Endogenous peroxidase was blocked for 20 min (1% hydrogen peroxide in methanol), and Ag retrieval was achieved using EDTA buffer. Then slides were incubated in horse serum for 20 min, followed by incubation in primary Abs CD3 (clone F7.2.38; DakoCytomation) and FoxP3 (clone 236A/E7; Abcam) and rabbit mAb to phosphoSTAT5 (Y694; Abcam) in blocking buffer (2% horse serum) for 60 min at 37°C in a humidified container for 1 h. The slides were washed in TBS/Tween (pH 7.6) for 5 min and incubated in Vector ImmPRESS Universal secondary kit (mouse anti-human and rabbit anti-human, Vector Laboratories, U.K.) for 30 min and diaminobenzidine substrate to visualize staining. Slides were counterstained in hematoxylin and mounted in DPX.

For double immunohistochemical staining, formalin-fixed paraffin-embedded tissue sections were dewaxed, rehydrated in TBS/Tween and blocked with endogenous peroxidase (as described above). Sections were subjected to Ag retrieval and incubated with 2% casein (Vector Laboratories) for 10 min. Primary mouse mAb, FoxP3 (clone 236A/E7, Abcam) was applied at a 1/50 dilution for 30 min. After a TBS/Tween wash, secondary ImmPRESS anti-mouse reagent (Vector Laboratories) was applied and visualized with ImmPACT diaminobenzidine (Vector Laboratories) for 5 min. Then sections were incubated again with 2% casein, followed by primary rabbit anti-human polyclonal CCL22 (Ab 53002, Abcam); secondary ImmPRESS rabbit anti-human reagent was applied, and visualization was performed with NovaRed substrate (both from Vector Laboratories). Sections were counterstained in hematoxylin, dehydrated through alcohol, placed into xylene, and mounted in DPX.

Sections for dual immunofluorescence were incubated with 10% normal mouse or rabbit serum for 30 min before adding the primary Abs against CCL22 or CD11c for 1 h. Control sections were incubated with IgG mouse mAb or rabbit IgG. Subsequently, sections were incubated with FITC or Texas Red secondary Abs for 30 min in the dark. Nuclei were counterstained with DAPI. Dual immunofluorescence was assessed using Axio Vision software.

Multicolor confocal microscopy

Liver tissue sections for NLs, diseased livers, and portal lymph nodes were incubated with blocking buffer (10% horse serum in PBS/1% BSA). Primary Abs against FoxP3, CD11c, CD3, and CD4 were applied for 1 h. FoxP3 primary Abs were amplified with anti-IgG1 biotin, followed by streptavidin Alexa Fluor 555 (Invitrogen). Rabbit monoclonal CD11c was

of $FoxP3^+$, $CD3^+$, and $CD4^+$ cells in inflamed liver (AIH and PBC shown as representative examples). *Right panel* shows magnification of *left panel*; arrow indicates costaining of Foxp3, CD3, and CD4. *B*, Multicolor confocal microscopy images of chronically inflamed liver compared with NL stained with mouse anti-human mAb to FoxP3 IgG1 (red), rabbit anti-human mAb to CD11c (green), and mouse anti-human mAb to CD8 IgG2b (blue). Cell nuclei stained with DAPI (gray). Staining was detected in PT, septa (*i*), and parenchyma (*ii*). *Top panel*, original magnification ×10 (scale bar, 200 μ); *bottom panel* original magnification ×40 (scale bar, 50 μ).*C*, Confocal images of $CD8^+$ (blue), FoxP3 (red), and CD11c (green) staining in a portal lymph node from a patient with PBC (*left panel*; representative staining from four experiments). The *right panel* (*i*) shows the magnified view (×40) of the boxed area in the *left panel* (×10). *D*, Flow cytometry dot-plot comparing the frequency of LIT_{regs} in normal and inflamed diseased liver (representative plots shown from eight diseased livers and seven NLs). LIT_{regs} were identified by gating on LILs $CD3^{high}CD4^{high}$, followed by $CD25^{high}$ (*y*-axis) and $CD127^{low}$ (*x*-axis). *E*, The ratio of $FoxP3^+$ cells to CD3-staining T cells was quantified by immunohistochemistry in NL and different chronic liver diseases. $p < 0.05$ comparing normal versus diseased livers; Mann-Whitney *U* test ($n = 8$). *F*, Percentage of $FoxP3^+$ cells in relation to CD3 in PT and parenchyma are shown for NL and different chronic liver diseases ($n = 7$).

Downloaded from http://www.jimmunol.org/ by guest on February 24, 2022

visualized by goat anti-rabbit FITC, then with rabbit anti-FITC, and, finally, with goat anti-rabbit FITC. CD8 and CD4 Abs were detected with anti-IgG2a Cy-3/IgG2b tetramethylrhodamine isothiocyanate (TRITC). All incubation steps were for 30 min, with 10-min washes in PBS, in a humidified chamber protected from the light. Quadruple immunofluorescence staining was visualized and analyzed by confocal microscopy using LSM software (ZEISS).

PCR and ELISA for CCL17 and CCL22

DCs and HSECs were stimulated with cytokines for 24 h, and cells and supernatant were stored for later analysis by RT-PCR and ELISA.

RT-PCR

LIDCs and MoDCs were stored in RNA later, and CCL17 and CCL22 gene expression was analyzed by RT-PCR amplification of RNA from LPS-stimulated and unstimulated LIDCs and MoDCs and from TNF-α + IFN-γ–stimulated and unstimulated HSEC low passage (passage two through four) and high passage (passage five and above).

Total RNA was extracted from cells using an RNeasy kit (Qiagen, Crawley, U.K.), and single-stranded cDNA was synthesized. The PCR reaction was conducted using hot start 95°C for 5 min, denaturing at 95°C for 3 min, annealing at 66°C, extension at 72°C for 33 cycles, and final extension at 72°C. Samples were stored at 4°C until used. Primers were designed from GenBank sequences for GAPDH, CCL17, and CCL22: GAPDH forward, 5′-GCC AAG GTC ATC CAT GAC AAC TTT GG-3′, reverse, 5′-GCC TGC TTC ACC ACC TTC TTG ATG TC-3′; CCL17 forward, 5′-ACT GCT CCA GGG ATG CCA TCG TTT TT-3′, reverse, 5′-ACA AGG GGA TGG GAT CTC CCT CAC TG-3′; and CCL22 forward, 5′-AGG ACA GAG CAT GGA TCG CCT ACA GA-3′, reverse, 5′-TAA TGG CAG GGA GGT AGG GCT CCT GA-3′. Product sizes for each set of primers were 270 bp for CCL17 and 363 bp for CCL22. Positive (MoDCs) and negative controls (no cDNA) were included in each assay. Amplified products were analyzed on a 2% agarose gel containing ethidium bromide (Sigma-Aldrich).

ELISA

Chemokines in cell culture supernatants (normalized to cell numbers) were measured by sandwich ELISA using Quantikine Human Immunoassay kits specific for human CCL17 (DDN00) and CCL22 (DMO00), according to the manufacturer's instructions (both from R&D Systems). All measurements were performed using triplicate samples for each experiment.

Multicolor flow cytometric analysis of matched blood T_{regs} and LIT_{regs}

We used freshly isolated LILs and matched PBLs for phenotypic analysis. Cells were washed, resuspended, and labeled for 45 min with different fluorochrome-labeled primary Abs against T_{reg} surface markers, phenotypic markers, and chemokine receptors at optimal dilutions at 4°C before washing with PBS 5% FCS. Following surface staining, cells were fixed in paraformaldehyde and permeabilized using a permeabilization buffer containing saponin (eBioscience, Cat00-5523), FoxP3 Ab conjugated to PE was used to detect intracellular FoxP3, and 2% rat serum was used to reduce background staining. Control samples were labeled with matched isotype control Abs. PBLs and LILs were gated using forward and side scatter parameters and then regated on CD3 and CD4. $CD25^{high}$, $CD127^{low}$, and $FoxP3^+$ were used to define T_{regs} and chemokine receptor expression, and immunophenotyping was done on this population.

To detect intracellular cytokines IFN-γ and TNF-α, LILs were stimulated again with 500 ng/ml ionomycin (Sigma-Aldrich) and/or 50 ng/ml PMA for 5 h in a 37°C incubator. The intracellular cytokine secretion was prevented using a Golgi block (brefeldin A, 1000 ng/ml). Cells were washed, and Abs were added in 100 μl permeabilization buffer. Samples were analyzed on a nine-color Dako Cyan Flow Cytometer using Summit 4.3 software (DakoCytomation).

Suppression of allogenic lymphocyte proliferation

Liver-infiltrating CD4 cells were isolated by negative selection and divided into $CD25^+CD4^+$ and $CD25^-CD4^+$ subsets by magnetic cell sorting. The ability of $CD25^+CD4^+$ cells (>95% purity by flow cytometry) to suppress proliferation was assessed by culturing liver-derived $CD25^+CD4^+$ lymphocytes with autologous naive lymphocytes, at ratios of 1:1 to 1:16, with added allogenic irradiated liver-derived DCs (1:100 ratio) or anti-human CD3/CD28 beads (DYNAL, Invitrogen) in 96-well round-bottom plates (Nunc, Rochester, NY). Suppression of proliferation was assessed by the incorporation of [^{3}H]thymidine. Cultures were pulsed with 1 μCi per well [^{3}H]thymidine (Amersham Biosciences) for the last 16 h of a 5-d incubation at 37°C in 5% CO_2, the plates were harvested, and proliferation was assessed by measuring radioactivity with a liquid scintillation counter. All cells were cultured in triplicate in a final volume of 200 μl RPMI 1640 with L-glutamine (2 mmol/l), 100 IU/ml penicillin, 100 IU/ml streptomycin, and 10% human AB serum.

Transwell chemotaxis of T_{regs}

The ability of LIT_{regs} to migrate to chemokines was assessed using 24-well plate transwells and fibronectin-covered (Sigma-Aldrich), 6.5-mm-diameter, 5-μm pore inserts (Corning). The lower chambers were filled with 600 μl assay media (RPMI 1640 medium with 0.1% BSA; Sigma-Aldrich) alone or supplemented with chemokines (100 ng/ml recombinant human CCL22 and CCL17, both from R&D Systems). Freshly isolated LIT_{regs} (5×10^5 in RPMI 1640) were added to the upper chamber. LIT_{regs} were collected from the top and bottom chambers after 4 h incubation at 37°C in 5% CO_2; the proportion of transmigrated cells was calculated by fixed-volume counting and phenotyped for T_{reg} markers and chemokine receptor expression by flow cytometry. Assays were conducted in duplicate and compared with control wells containing RPMI 1640 medium with 0.1% BSA alone. T_{regs} were incubated with pertussis toxin (PTx; 100 ng/ml; Sigma-Aldrich) prior to the assay to inhibit chemokine-mediated signaling.

Flow-based transendothelial migration assay

We performed a flow-based adhesion assay incorporating HSECs grown in microslides to study interactions between human HSECs and freshly isolated T_{regs} under physiological blood flow (18, 22). HSECs were cultured to confluence in glass microslides, stimulated for 24 h with TNF-α and IFN-γ (both 10 ng/ml; PeproTech), and connected to the flow-based system, as described previously (22). Freshly isolated T_{regs} were perfused through microslides at flow rates of 0.182 ml/min, generating shear stresses of 0.05 Pa, which are comparable to wall shear stresses found in the liver sinusoids in vivo. Adherent cells were visualized microscopically under phase contrast, and a video monitor was used to record assays for off-line analysis to determine the percentage of rolling cells, statically adherent cells, and transmigrated cells. The number of adherent cells was converted to adherent cells/mm^2 corrected for the number of T_{regs} perfused (i.e., adherent cells/mm^2 per 10^6 T_{regs} perfused). Cells appearing phase bright were above the endothelial monolayer, whereas those appearing phase dark had migrated through the monolayer. HSEC monolayers were incubated with blocking Abs against ICAM-1 (11C81: 10 μg/ml) and VCAM-1 (4B2: 10 μg/ml) (both from R&D Systems), or lymphocytes were incubated with a blocking Ab raised against CXCR3 (MAB160/49801; 10 μg/ml; R&D Systems;) for 30 min. To inhibit chemokine-mediated signaling, T_{regs} were incubated with PTx (100 ng/ml; Sigma-Aldrich) 30 min prior to assay. We also blocked the individual CXCR3 chemokine ligands by incubating HSECs with anti-CXCL9 (49106; 50 μg/ml), anti-CXCL10 (33036; 5 μg/ml), or anti-CXCL11 (87328; 5 μg/ml) (all from R&D Systems) for 30 min. HSECs had been stimulated for 24 h with TNF-α and IFN-γ to induce the expression of CXCR3 ligands.

All experiments were compared with control microslides in which isotype-matched IgG was used.

Statistical analysis

Paired or independent *t* tests were used to assess data that were normally distributed, whereas nonparametric data were compared using the Mann-Whitney *U* test.

Results

Definition of LIT_{regs} and peripheral blood-derived regulatory T cells

Liver and blood-derived T_{regs} were defined by the characteristic phenotype $CD4^+CD25^{high}CD127^{low}FoxP3^+$ (8, 9). Liver-derived lymphocytes were freshly isolated from explanted human liver tissue by mechanical digestion and density gradient centrifugation before being stained with Abs against CD3, CD4, CD25, CD127, and the intracellular transcription factor FoxP3. More than 95% of $CD4^+CD25^{high}CD127^{low}$ LILs expressed FoxP3 (Fig. 1*A*). The vast majority of LIT_{regs} expressed CD45RO, and >80% expressed high levels of CD27 (Fig. 1*B*), consistent with a tissue-infiltrating phenotype. More than 90% of LIT_{regs} expressed the surface ectoenzyme CD39, and 35% expressed OX-40 (Fig. 1*B*).

Downloaded from http://www.jimmunol.org/ by guest on February 24, 2022

LIT_{regs} suppress T cell activation in vitro

Allogenic stimulation/suppression assays confirmed that LIT_{regs} suppress T cell activation in vitro at ratios of 1:4 T_{reg}/responder cells, demonstrating that LIT_{regs} are functional (Fig. 1*C*).

Chronically inflamed human liver tissue contains a higher proportion of LIT_{regs} than nondiseased liver

Few T_{regs} were detected in NL tissue by immunohistochemistry, although they could be readily detected in the chronically inflamed livers (Fig. 2*A*) in septal and parenchyma areas (Fig. 2*A*, 2*B*). Multicolor confocal microscopy staining revealed them to be closely associated with CD8 T cells and CD11c DCs (Fig. 2*B*). T_{regs} were also detected in liver-draining portal lymph nodes in close association with $CD8^+$ cells and $CD11c^+$ DCs (Fig. 2*C*). T cells were readily isolated from normal and inflamed liver tissue (Fig. 2*D*), and the total numbers and the proportion of the infiltrate that was $CD4^+CD25^{high}CD127^{low}FoxP3^+$ was greater in diseased tissue than in NL tissue (Fig. 2*D*). We used immunohistochemistry to quantify the proportion

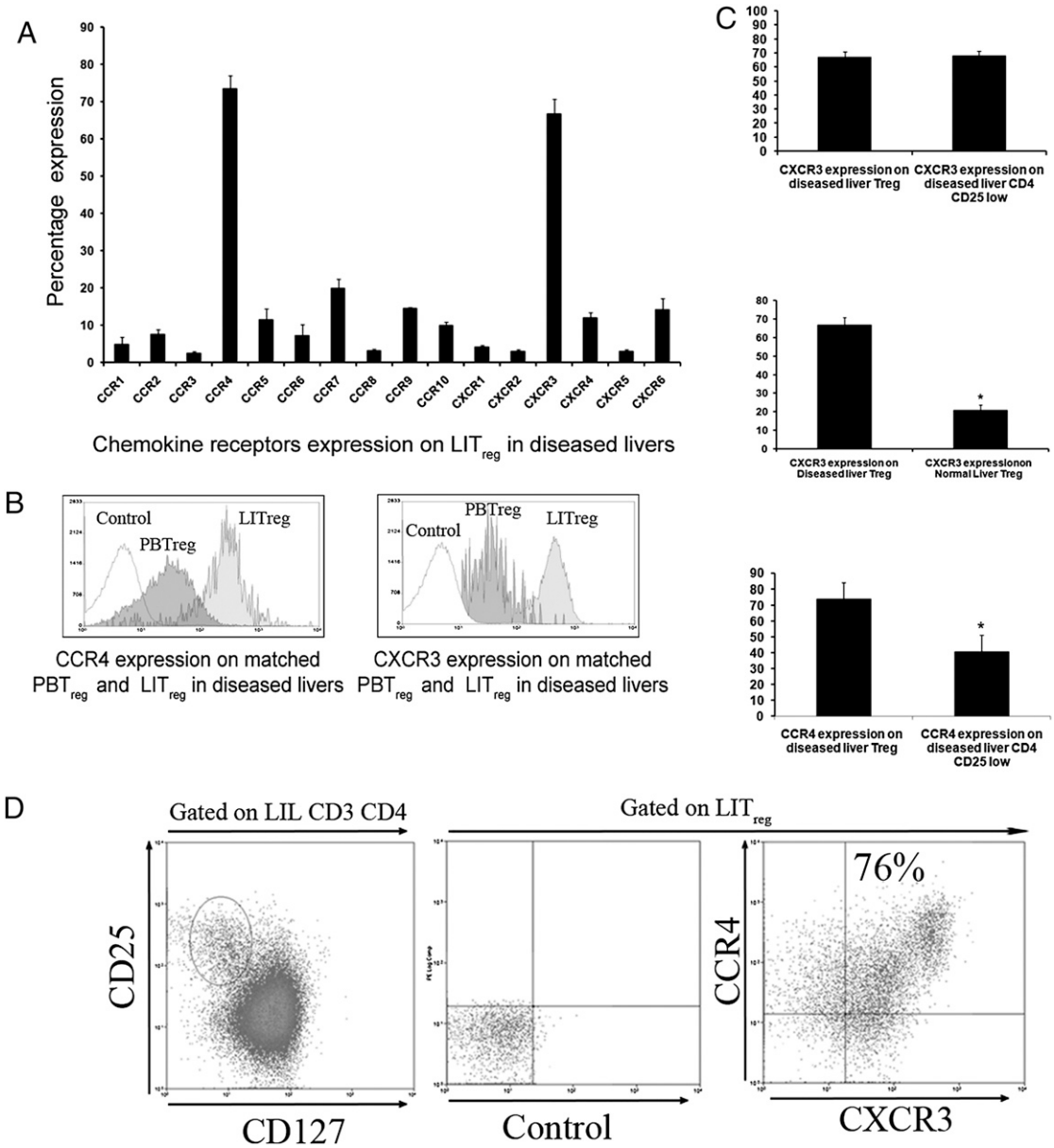

FIGURE 3. Chemokine receptor expression on LIT_{regs}. *A*, Flow cytometry was used to analyze staining for chemokine receptors on liver-infiltrating $CD4^{high}CD25^{high}CD127^{low}FoxP3^+$ T_{regs} freshly isolated from diseased liver tissues. The chemokine receptors CCR1-10 and CXCR1-6 were stained together with T_{reg} markers, and the percentage of cells expressing each chemokine receptor was analyzed. Data represent mean ± SEM of seven different experiments using livers from patients with ALD, PBC, cryptogenic cirrhosis, AIH, seronegative (non-A non-B) hepatitis, and chronic hepatitis C. *B*, Overlay graph of CCR4 and CXCR3 frequency on LIT_{regs} from inflamed liver tissue compared with peripheral blood T_{regs} (PBT_{regs}) in matched samples from patients who underwent liver transplantation. Cells were gated on $CD4^{high}CD25^{high}CD127^{low}FoxP3^+$. One representative graph of five experiments from a patient with PBC. *C*, Analysis of CXCR3 expression on freshly isolated $CD4^{high}CD25^{high}LIT_{regs}$ compared with $CD4^{high}CD25^{low}$ cells from diseased livers (*top panel*), CXCR3 expression on diseased $CD4^{high}CD25^{high}LIT_{regs}$ compared with normal $CD4^{high}CD25^{high}$ LIT_{reg} (*middle panel*), and CCR4 expression on $CD4^{high}$ $CD25^{high}$ LIT_{regs} compared with $CD4^{high}CD25^{low}$ cells from diseased liver (*bottom panel*). LILs were gated on T_{reg} markers, CD4, CD25, and $CD4CD25^{high}$; $CD4CD25^{low}$ gating was applied to CXCR3 and CCR4 expression. Data represent mean ± SEM ($n = 5$). $*p < 0.05$, Student *t* test. *D*, CCR4 and CXCR3 are coexpressed on LIT_{regs}. LILs gated on $CD3^+CD4^+CD127^{low}CD25^{high}$ were stained for CCR4 (*y*-axis) and CXCR3 (*x*-axis), confirming the coexpression of these chemokine receptors on the same cell. One representative experiment of five is shown from a patient with AIH.

Downloaded from http://www.jimmunol.org/ by guest on February 24, 2022

of the CD3 infiltrate that was FoxP3$^+$ in a variety of liver diseases. In all diseases studied, the inflamed diseased liver contained a higher proportion of T_{regs} compared with nondiseased liver (Fig. 2*E*). Interestingly, greater numbers of T_{regs} were seen in the patients with the most severe inflammation, with the highest frequencies detected in patients who had undergone emergency liver transplantation for fulminant liver failure as a consequence of severe seronegative (non-A non-B) hepatitis (Fig. 2*E*). In seronegative hepatitis and AIH, FoxP3$^+$ T_{regs} were found at higher frequencies in the parenchyma compared with PTs, whereas in the other liver diseases and in NL, FoxP3$^+$ T_{regs} were detected at higher frequencies in PTs (Fig. 2*F*)

LIT_{regs} express high levels of CXCR3 and CCR4

The results of staining for chemokine receptor expression on freshly isolated liver-derived T_{regs} are shown in Fig. 3*A*. Approximately 20% ± 5% of LIT_{regs} expressed CCR7, but the majority expressed CCR4 (74% ± 7%) and CXCR3 (67 ± 9% SD) (Fig. 3*A*). Furthermore, the levels of these receptors were higher on LIT_{regs} isolated from inflamed liver compared with NL tissue: 74% ± 7%% versus 32% ± 7% for CCR4 and 67% ± 9% versus 21% ± 6% for CXCR3 ($p \leq 0.05$ for both) (Fig. 3*C*). We compared levels of CCR4 and CXCR3 in circulating and liver-derived T_{regs} of patients from whom we had collected matched blood and liver samples (Fig. 3*B*): 82% of LIT_{regs} stained for CCR4 versus 67% of matched blood T_{regs}, and 66% of LIT_{regs} stained for CXCR3 compared with 43% of matched blood T_{regs} ($p < 0.05$). Seventy-four percent of LIT_{regs} expressed CCR4, compared with 40% of liver-infiltrating CD4$^+$ CD25^{low} cells from diseased livers. Thus, CCR4 is preferentially expressed on LIT_{regs}. However, the levels of CXCR3 were similar for LIT_{regs} and liver-infiltrating CD4$^+$CD25^{low} cells (Fig. 3*C*).

We correlated CCR4 with CXCR3 expression on LIT_{regs} to determine whether the receptors were coexpressed on the same cells or whether there were two subpopulations of LIT_{regs} defined by CCR4 and CXCR3 expression (Fig. 3*D*). More than 75% of LIT_{regs} coexpressed CCR4 and CXCR3 (Fig. 3*D*), and 40% of the residual LIT_{regs} that were CCR4$^+$ but CXCR3^{low} coexpressed CCR4 and CCR5 (data not shown).

CXCR3 activation promotes stable adhesion and transmigration of LIT_{regs} across human HSECs under conditions of flow

Cultured HSECs express markers that are characteristic of sinusoidal endothelium in vivo, including CD31, lymphatic vessel

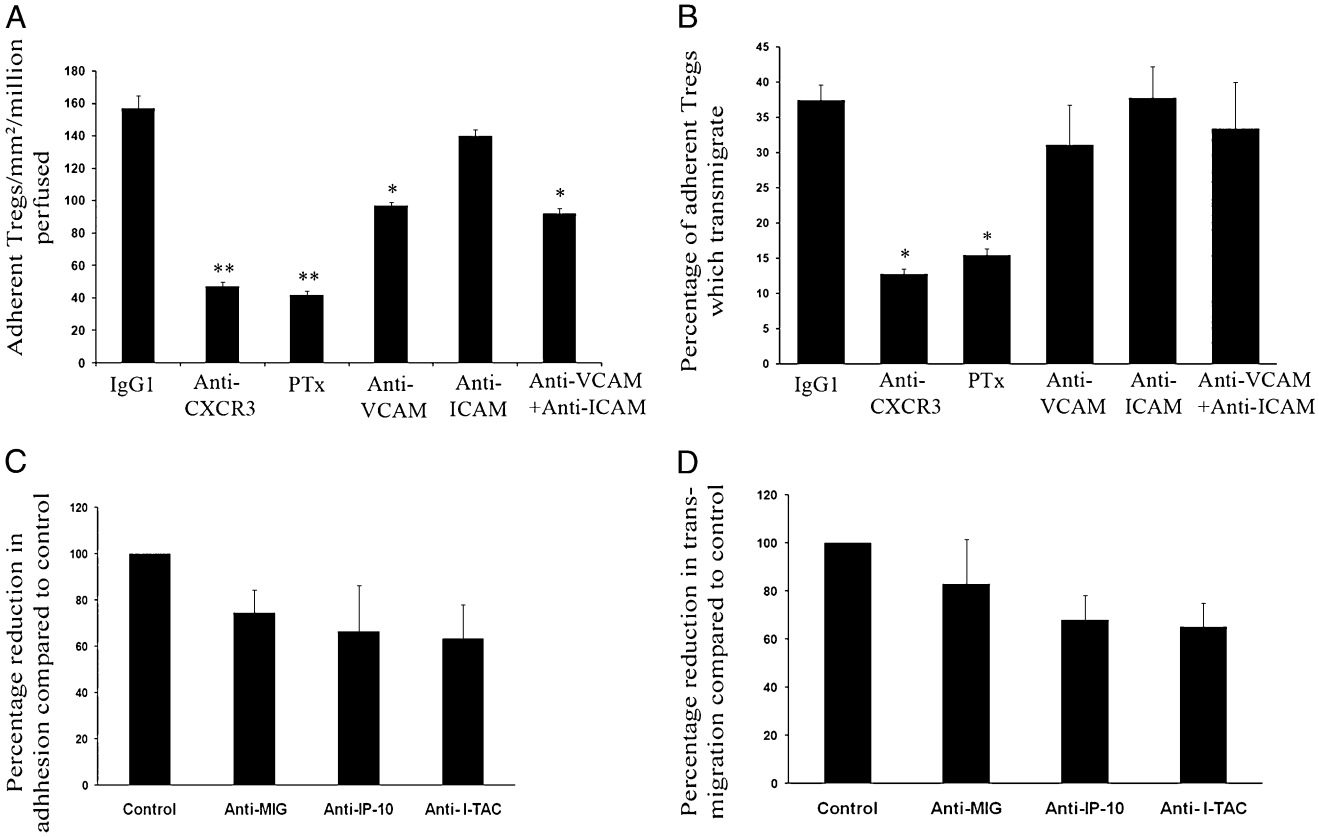

FIGURE 4. T_{reg} adhesion and transmigration across activated HSECs is dependent on CXCR3 and VCAM-1. *A*, Effect of Gi protein inhibition using PTx and Ab inhibition of CXCR3 or VCAM-1 on total adhesion of T_{regs}. Flow-based adhesion was done with freshly isolated T_{regs} flowed across 24-h TNF-α– and IFN-γ–stimulated primary human HSECs. Data represent the number of adherent T_{regs}/mm^2/million perfused (mean ± SEM of five experiments). $*p < 0.05$; $**p < 0.005$. Statistical significance was calculated using paired *t* tests, comparing treatment with control. All experiments were performed at 0.05 Pa, which is similar to the shear stress in hepatic sinusoids in vivo. *B*, Transmigration of adherent T_{regs} through the same stimulated HSECs. Migrating cells were calculated using frame-by-frame analysis of experimental videos to count the percentage of phase dark (transmigrated) T_{regs}. All experiments were performed at 0.05 Pa. Data shown as percentage of adherent T_{regs} that had transmigrated (mean ± SEM of five experiments). $*p < 0.05$; paired *t* tests comparing treatment with control. *C*, Effect of blocking individual CXCR3 ligands on total adhesion of T_{regs}. To investigate the individual effect of CXCR3 ligands, anti-CXCL9, anti-CXCL10, and anti-CXCL11 were used to block individual CXCR3 ligands on 24-h TNF-α– and IFN-γ–stimulated primary human HSECs. Adhesion was calculated using frame-by-frame analysis of experimental videos to count the percentage of cells adherent to HSECs. Percentage reduction in adherent T_{regs} to stimulated endothelium with individual chemokine blockade was compared with control. Data represent mean ± SEM of four experiments. All experiments were carried out at 0.05 Pa. *D*, Effect of blocking individual CXCR3 ligands on transmigration of T_{regs}. Transmigration was calculated using frame-by-frame analysis of experimental videos to count the percentage of cells that migrated through HSECs (phase dark). The percentage reduction in transmigration of adherent T_{regs} to stimulated endothelium with individual chemokine blockade was compared with control. Data represent mean ± SEM of four experiments.

Downloaded from http://www.jimmunol.org/ by guest on February 24, 2022

endothelial receptor 1, liver/lymph node-specific intercellular adhesion molecule-3-grabbing integrin, and liver and lymph node sinusoidal endothelial cell C-type lectin (23–25). When stimulated by TNF-α, HSECs express ICAM-1 and VCAM-1 and support the adhesion of lymphocytes under conditions of flow (22). Furthermore, HSECs secrete the CXCR3 ligands CXCL9, CXCL10, and CXCL11 in response to IFN-γ; this is increased if TNF-α is used in combination with IFN-γ (18). Thus, we used HSECs treated with 10 ng/ml IFN-γ and TNF-α in the flow-based adhesion assays in the current study to allow us to model inflamed hepatic sinusoidal endothelium, which expresses ICAM-1, VCAM-1, and CXCR3 ligands in chronic hepatitis (18).

When flowed over cytokine-stimulated HSECs, some of the T_{regs} displayed brief rolling/tethering interactions followed by arrest and stable adhesion, whereas others arrested without rolling; this behavior was similar to that reported using unfractionated liver-derived lymphocytes (18). The numbers of cells undergoing stable adhesion from flow could be reduced by blocking CXCR3 and, to a lesser extent, VCAM-1 but not by blocking ICAM-1. Global Gα protein inhibition with PTx reduced adhesion to levels seen with anti-CXCR3 blockade, suggesting that CXCR3 is the dominant chemokine receptor involved (Fig. 4*A*). The proportion of adherent cells that subsequently underwent transendothelial migration was also significantly reduced by CXCR3 block. Again, PTx had a similar inhibitory effect to CXCR3 blockade.

These findings suggest that CXCR3 is crucial for T_{reg} adhesion to, and subsequent transmigration across, inflamed hepatic sinusoids (Fig. 4*B*). To determine which of the CXCR3 ligands is involved,

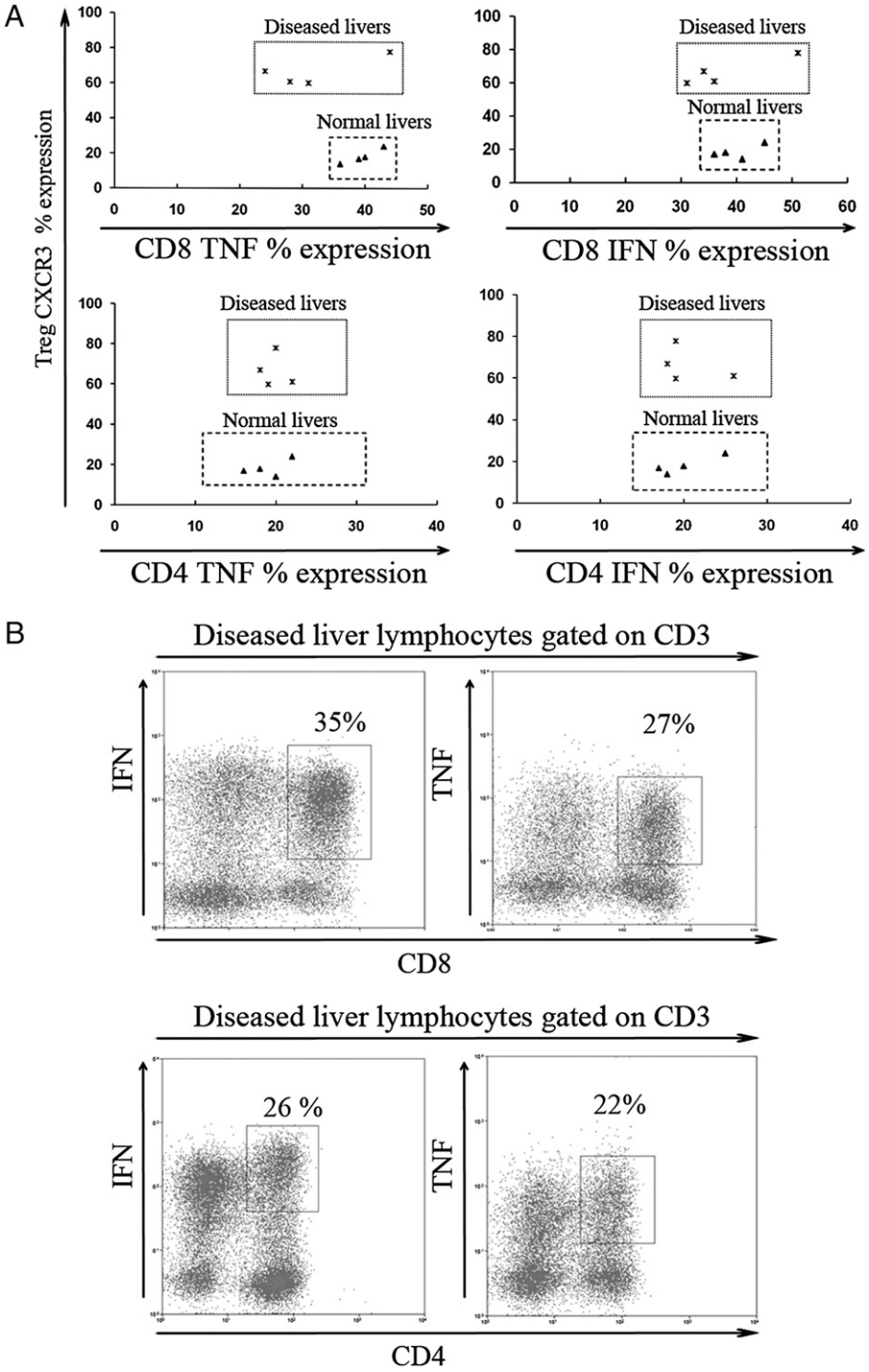

FIGURE 5. LIT_{reg} CXCR3 expression and liver-infiltrating CD4 and CD8 effector cell cytokine expression. To determine whether the levels of CXCR3 expression by LIT_{regs} are associated with secretion of TNF-α and IFN-γ by liver-infiltrating CD4 and CD8 effector cells, we correlated levels of CXCR3 expression on LIT_{regs} with the frequency of IFN-γ– and TNF-α–secreting effector cells in the same liver samples. *A*, The percentage of liver-derived CD8 (*upper panel*) and CD4 (*lower panel*) T cells expressing TNF-α (*left panels*) and IFN-γ (*right panels*) is shown on the *x*-axis, and the frequency of $CXCR3^+$ T_{regs} ($CD4^+$ $CD25^{high}CD127^{low}$) isolated from the same donor liver and analyzed without expansion is shown on the *y*-axis. Cells from four NLs and four diseased livers (AIH, PBC, ALD, and non-A non-B [seronegative] fulminant hepatitis) are shown. There was no clear correlation between CXCR3 frequencies in the T_{reg} population and cytokine secretion by effectors. Intracellular cytokine and TNF-α and IFN-γ staining was done by incubating LILs with PMA and ionomycin for 5 h, with brefeldin A Golgi block in the last 2 h, followed by intracellular cytokine staining. The patient with the highest frequency of TNF-α– and IFN-γ–secreting effector cells had fulminant non-A non-B hepatitis. *B*, A representative flow cytometry dot-plot analysis of T cells isolated from a diseased liver (PBC) is shown to demonstrate IFN-γ and TNF-α secretion. Cells were gated on LILs and gated again on CD3 lymphocytes (one representative example of four experiments).

Downloaded from http://www.jimmunol.org/ by guest on February 24, 2022

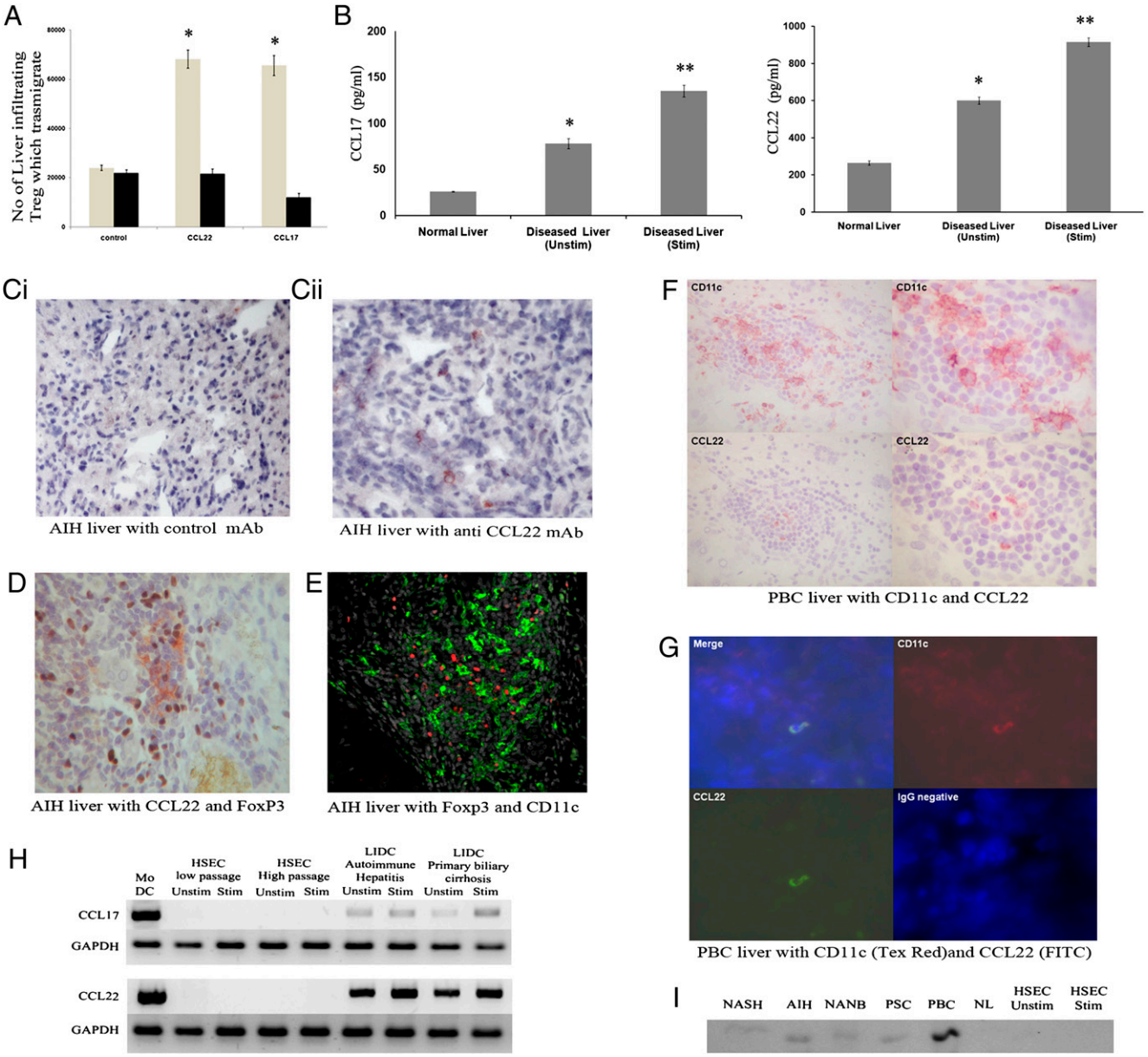

FIGURE 6. CCR4 ligands are detected in diseased liver tissue and secreted by LIDCs. *A*, LIT_{regs} migrate toward CCR4 ligands in vitro. Migration of LIT_{regs} to CCR4 ligands CCL22 and CCL17 was assessed using fibronectin-coated 5-μm-pore transwell migration chambers. The lower chambers were filled with 600 μl assay media (RPMI 1640 medium with 0.1% BSA) alone or supplemented with chemokines (100 ng/ml recombinant human CCL22 and CCL17). BSA was used as control. A total of 5×10^5 T_{regs} isolated from inflamed livers ($n = 4$) were loaded per well in the upper chamber; T_{regs} were collected from the top and bottom chambers after 4 h of incubation at 37°C in 5% CO_2. The proportion of transmigrated cells was calculated by fixed-volume counting and phenotyped for T_{reg} markers and chemokine receptor expression by flow cytometry. To inhibit chemokine-mediated signaling, T_{regs} were incubated with PTx (100 ng/ml) prior to the assay. Results are expressed as mean ± SEM. LIT_{regs} showed significant migration responses to CCL22 and CCL17 compared with migration to BSA, and these were inhibited by PTx. $*p < 0.05$, Student *t* test. *B*, To determine whether liver DCs secrete CCL17 and CCL22, we isolated and cultured myeloid DCs from human liver tissue and stimulated them with LPS (1 μg/ml) for 24 h. CCL17 and CCL22, measured by ELISA, were detected in cell culture supernatants of LPS-stimulated liver-derived DCs isolated from patients with AIH ($n = 2$) or PBC ($n = 1$) or from NL ($n = 3$). All DCs secreted detectable CCL17 and CCL22, with a >2-fold increase in secretion by DCs derived from inflamed liver tissue compared with NL. Data represent mean ± SEM of three experiments using supernatants from different DCs. Values represent the chemokine concentration (pg/ml) of three replicate wells relevant to a standard curve of known concentration. $*p \leq 0.05$; $**p \leq 0.01$. *C*, Expression of CCL22 in human liver tissue samples by immunohistochemistry. CCL22 staining (*i*) was detected on LIDCs within inflammatory infiltrates (positive staining cells brown) in a patient with AIH. No detectable CCL22 was found in NL or when control Abs were used (*ii*). (Original magnification ×200.) *D*, Dual staining of FoxP3-expressing cells (brown) and CCL22 (red) in liver tissue from a patient with AIH reveals $CCL22^+$ cells in close association with $FoxP3^+$ T_{regs} within an inflammatory infiltrate (original magnification ×200). *E*, Confocal image of dual staining of FoxP3-expressing cells (red/TRITC) and CD11c (green/FITC) in liver tissue from a patient with AIH reveals $CD11c^+$ cells in close association with $FoxP3^+$ T_{regs} within an inflammatory infiltrate (original magnification ×40). *F*, Colocalization of DCs and CCL22 in inflamed liver tissue. Serial liver sections from a patient with PBC were stained with CD11c (*top panels*) and CCL22 (*bottom panels*). Cells that coexpress CD11c and CCL22 can be determined by comparing staining of CD11c (*top right panel*) and CCL22 (*bottom right panel*) at higher power (original magnification ×200). Staining with isotype-matched control Abs was negative (*left panels*, original magnification ×100.) *G*, Colocalization of DCs and CCL22 in inflamed liver tissue. Staining of FITC-labeled CCL22 (green) with Texas Red-labeled CD11c (red). Areas of coexpression (*top left panel*) appear yellow. Nuclei were stained with DAPI (blue). Control Abs demonstrated minimal background tissue fluorescence. The findings are representative of the pattern of immunofluorescence staining seen in tissue sections from four donors each for PBC, ALD, AIH, and HCV

Downloaded from http://www.jimmunol.org/ by guest on February 24, 2022

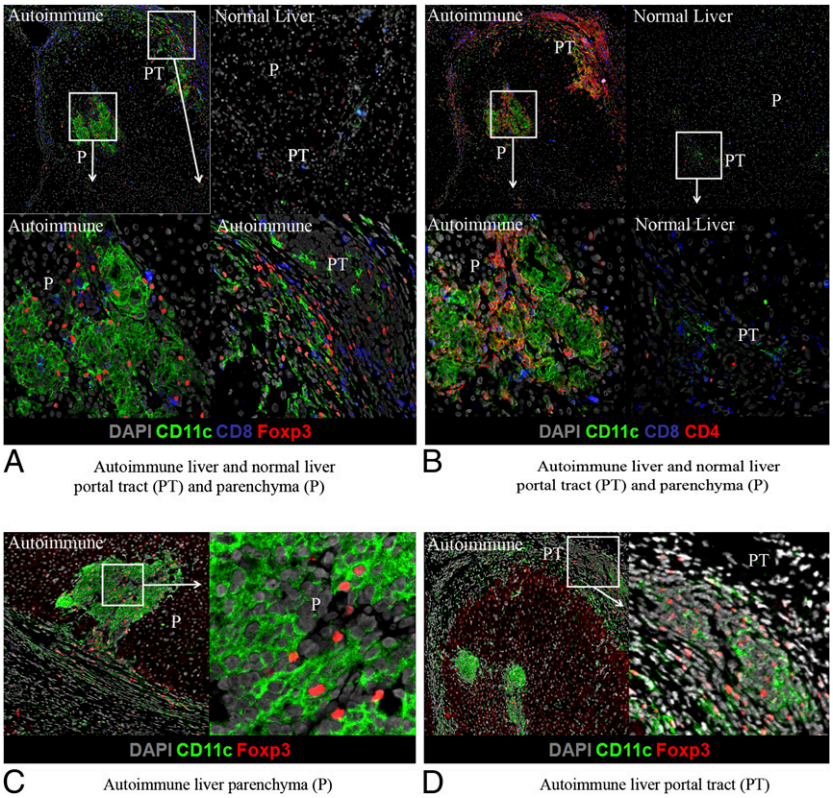

FIGURE 7. Close proximity of T_{regs}, T effectors, and DCs in parenchyma and PT of normal and inflamed liver. *A*, Quadruple-color confocal images of inflamed liver PT and parenchyma (P) showing LI-T_{regs} in chronically inflamed liver (AIH liver; *top left panel*) as an example compared with NL (*top right panel*). *Lower panels* show the magnification of parenchyma (P) and PT areas (stains: FoxP3 T_{regs}, TRITC [red]; CD8, Cy5 [blue]; CD11c, FITC [green]; cell nuclei, DAPI [gray]) (original magnification: *upper panels*, ×25; *lower panels*, ×40). *B*, Quadruple-color confocal microscopy images of $CD11c^+$ DCs and T effector cells (CD4 and CD8) in inflamed PT and parenchyma (P) in a patient with autoimmune liver disease (*left panels*) and NL (*right panels*). CD4 (TRITC [red]) and CD8 (Cy3 [blue]) DCs are detected in close proximity with $CD11c^+$ DCs (FITC [green]) (original magnification: *upper panels*, ×25; *lower panels*, ×40). Three-color confocal staining images of autoimmune liver hepatic parenchyma (P) infiltrate (interface hepatitis) (*C*) and PT (*D*) showing FoxP3 (TRITC [red]) and CD11c (FITC [green]) cell types are closely associated in infiltrates in the inflamed parenchyma lobules (P) and PT. Cell nuclei are stained with DAPI (gray).

we repeated the experiments using blocking Abs against the individual CXCR3-binding chemokines CXCL9 (monokine induced by IFN-γ), CXCL10 (IFN-γ inducible protein-10), and CXCL11 (IFN-inducible T cell α-chemoattractant). We observed a reduction in adhesion (Fig. 4*C*) and transmigration (Fig. 4*D*) with each individual blocking Ab treatment, but these were less than the inhibition seen with anti-CXCR3, which suggests that all three ligands may be involved. This is consistent with our previous work showing that HSECs secrete all three ligands in response to IFN-γ and TNF-α (18).

Correlation between CXCR3 expression on LIT_{regs} and cytokine secretion by liver-infiltrating effector T cells

To determine whether proinflammatory cytokines secreted by liver-infiltrating effector cells are responsible for activating the CXCR3 pathway, we investigated whether the levels of CXCR3 expression on T_{regs} correlated with IFN-γ and TNF-α secretion by effector cells in the same livers. NL and inflamed liver contained IFN-γ– and TNF-α–secreting CD4 and CD8 T cells (Fig. 5*B*). The proportion of cytokine-expressing cells was similar in normal and diseased tissue, although the total number of T cells was much higher in the inflamed livers. Once again, we detected higher frequencies of $CXCR3^+$ T_{regs} in inflamed liver tissue (60–80% cells positive) compared with those isolated from nondiseased liver (15–28%) (Fig. 5*A*). However, there was no correlation between CXCR3 expression on T_{regs} and the proportion of CD4 or CD8 TNF-α– and IFN-γ–secreting cells in the infiltrate (Fig. 5*A*).

LIT_{regs} express functional CCR4

We used chemotaxis assays to confirm that CCR4 on LIT_{regs} is functional, as demonstrated by the ability of the cells to migrate to the CCR4 ligands CCL17 and CCL22 (Fig. 6*A*). The chemotactic indices for CCL17 and CCL22 were approximately three times greater than control. We phenotyped the LIT_{regs} before chemotaxis assays and confirmed that >75% expressed CCR4.

Localization and source of CCR4 ligands CCL17 and CCL22 in inflamed liver tissue

We were unable to detect CCL17 and CCL22 in NL tissue, but both chemokines were detected in chronically inflamed liver tissue by Western blotting (Fig. 6*I*) and immunohistochemistry (Fig. 6*Cii*, 6*D*, 6*F*). Immunohistochemistry demonstrated that CCL22 is present in cells with the morphology of DCs in inflamed liver tissue (Fig 6*Cii*, 6*D*, 6*F*). Staining was most marked at areas of active inflammation, including portal infiltrates, interface hepatitis, and lobular hepatitis within the parenchyma (Fig. 6*Cii*, 6*D*). There was no detectable staining of DCs with isotype-matched control Abs (Fig. 6*Ci*). Confocal staining showed that intrahepatic $CCL22^+$ DCs were closely associated with LIT_{regs} in PTs and inflamed parenchyma (Fig. 6*E*, Fig. 7) and in close proximity to CD4 and CD8 T cells (Fig. 7). Serial liver sections (Fig. 6*F*) and

(original magnification × 200). *H*, De novo synthesis of CCR4 ligands CCL17 and CCL22 by liver-derived DCs was confirmed by RT-PCR. LIDCs isolated from liver tissue from patients with AIH and PBC were analyzed unstimulated or after stimulation with LPS. Monocyte-derived TNF-α–activated DCs (MoDCs) are shown as a positive control, and unstimulated and stimulated HSECs were used as a negative control. CCL17 and CCL22 mRNA was detected in LIDCs. Representative data from one of three experiments is shown. *I*, Western blot analysis of CCL17 in liver tissue lysates from different chronic liver diseases and unstimulated or TNF-α/IFN-γ–stimulated HSEC lysates. CCL17 is present in chronically inflamed diseased livers, but it could not be detected in NL tissue lysates or in lysates of HSECs. One representative blot of five experiments is shown. HSEC Unstim, unstimulated HSECs; HSEC Stim, HSECs stimulated with TNF-α and IFN-γ; NANB, non-A non-B seronegative hepatitis; NASH, nonalcoholic steatohepatitis; PSC, primary sclerosing cholangitis.

Downloaded from http://www.jimmunol.org/ by guest on February 24, 2022

dual staining (Fig. 6*G*) suggested that CCL22 expression was detected on CD11c DCs in inflamed liver.

Liver-derived DCs secrete CCL17 and CCL22

To confirm that hepatic DCs secrete CCR4 ligands, we isolated myeloid DCs from normal and inflamed human liver tissue and analyzed them for the expression of CCL17 and CCL22. mRNA (Fig. 6*H*) and protein (Fig. 6*B*) for both chemokines were detected in DCs isolated from diseased liver; neither mRNA (Fig. 6*H*) nor protein (Fig. 6*I*) could be detected in HSECs, even after cytokine stimulation consistent with the lack of detectable CCL17 and CCL22 on sinusoids by immunohistochemistry (Fig. 6*Cii*, 6*D*). Furthermore, we localized staining of CCL22 to LIDCs in liver tissue (Fig. 6*G*). These data are consistent with previous reports that myeloid DCs secrete CCL17 and CCL22 when stimulated with LPS (26).

The majority of LIT_{regs} do not express phosphoSTAT5

We looked for evidence of STAT5 activation in LIT_{regs} by staining liver tissue with an Ab that recognizes phosphoSTAT5 (Fig. 8). PhosphoSTAT5 was detected in <20% of the $FoxP3^+$ cells, suggesting that not all FoxP3 T_{regs} are actively signaling through IL-2R (Fig. 8).

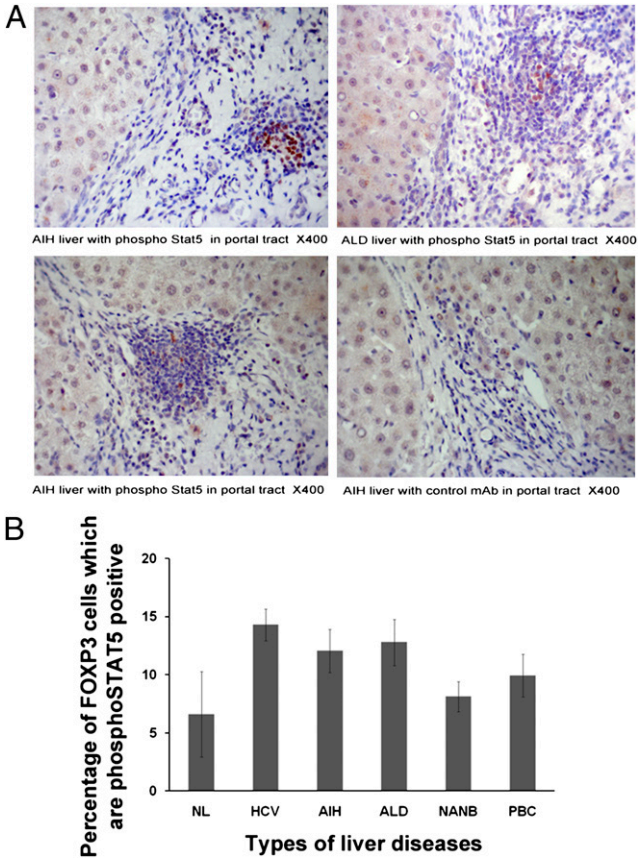

FIGURE 8. Detection of phosphoSTAT5 in inflamed human livers. *A*, Single immunohistochemical staining of formalin-fixed, paraffin-embedded liver sections showed phophoSTAT5 staining using mAbs (detected as a brown pigment) in PT and parenchyma (P) of patients with AIH or ALD. Control sections were stained with isotype-matched IgG Abs, and staining was negative (original magnification ×400). *B*, The percentage of phosphoSTAT5-positive FoxP3 cells in normal and inflamed livers. Paraffin-embedded serial liver sections were stained with FoxP3 mAbs and phosphoSTAT5 Abs; the numbers of cells with positive staining were counted from the same areas, and the percentage positivity of phosphSTAT5 in relation to FoxP3 was calculated. $n = 6$ each for diseased livers and NL.

Discussion

T_{regs} operate at sites of inflammation in peripheral organs as well as in secondary lymphoid tissues (12, 27). At inflammatory sites, they mediate bystander and Ag-specific suppression of local immune responses to prevent collateral tissue damage in response to injury and infection (28–30). The outcome of chronic inflammation is the result of a balance between pro- and anti-inflammatory responses in which T_{regs} maintain stable chronic inflammation while preventing fulminant destructive inflammation (31). This is particularly important in liver disease, in which intrahepatic T_{regs} are detected in chronic hepatitis from a variety of causes (5, 32, 33). The frequency and function of intrahepatic T_{regs} were reported to affect the outcome of chronic infection with hepatitis B and C viruses and to be associated with suppression of the antitumor immune response in hepatocellular carcinoma (4, 33).

We found low numbers of T_{regs} in nondiseased human liver and a higher number in the liver of patients with a variety of autoimmune and chronic inflammatory liver diseases. Approximately 5% of the CD3 T cells in NL tissue expressed FoxP3 by immunohistochemistry; this proportion was significantly greater in chronic inflammatory liver diseases. We also isolated $CD4^+CD25^+FoxP3^+CD127^{low}$ cells from explanted liver tissue and again found that NL contained low frequencies of T_{reg} and that the frequencies were increased in chronic inflammatory liver diseases. The proportion of liver-derived T cells that stained $CD4^+CD25^+FoxP3^+CD127^{low}$ after isolation from liver tissue was lower than the proportion seen in situ using immunohistochemistry with Abs to FoxP3. This could be because FoxP3 stains other cells in liver tissue, although this seems unlikely because the majority of $FoxP3^+$ liver-derived lymphocytes were $CD4^+CD25^+CD127^{low}$. Alternatively, our tissue-isolation methods may not remove all of the LIT_{regs}. However, although the proportions of T_{regs} varied using the two methods, the overall results were similar, with the highest frequencies detected in patients with fulminant seronegative (non-A non-B) hepatitis, the most florid and destructive form of hepatitis that leads to liver failure. These findings suggest that T cell-mediated hepatitis and liver destruction are not a consequence of the failure of T_{regs} to infiltrate the liver but rather are due to an inability of the recruited cells to control the effector arm of the response.

Analysis of the distribution of T_{regs} in liver tissue demonstrated them to be closely associated with $CD11c^+$ DCs and CD8 T cells at sites of inflammation in PTs and in the hepatic lobules. Thus, T_{regs} are ideally situated to mediate suppression of intrahepatic immune responses. To confirm that they were functional, we isolated $CD4^+CD25^+FoxP3^+CD127^{low}$ cells from liver tissue and showed that they suppressed T cell activation in vitro. These cells were $CD27^{high}$, consistent with previous reports that CD27 expression characterizes tissue-infiltrating T_{regs} in inflamed synovial tissue1 (13).

The migration and positioning of leukocytes in tissues during homeostasis and in response to inflammation are controlled by the coordinated expression of adhesion molecules and chemokine receptors that determine where and when cells will be recruited via endothelium, as well as their subsequent migration and positioning in tissue. Little is known about the molecular control of T_{reg} recruitment to inflamed tissues, although this will be critical in defining their role in disease and in developing strategies for their therapeutic use. To determine the receptors responsible for the recruitment of T_{regs} to human liver, we compared chemokine receptor expression on liver-derived T_{regs} (analyzed without expansion straight from liver tissue) with blood-derived T_{regs} isolated from the same patient at the time of liver transplantation. In particular, two receptors were overexpressed

Downloaded from http://www.jimmunol.org/ by guest on February 24, 2022

on liver-infiltrating cells: CXCR3 and CCR4; the majority of LIT_{regs} in chronic inflammatory liver diseases express both receptors.

CXCR3 was reported on circulating human T_{regs} (34, 35), where its expression is presumed to favor homing to inflamed tissue sites. Our data confirm that this is the case because the majority of T_{regs} in inflamed human liver expressed high levels of functional CXCR3, which promoted their transmigration across liver endothelium under flow. We found that only 15–20% of T_{regs} in NL expressed CXCR3, which further supports its particular role in the recruitment of T_{regs} to sites of inflammation. Levels of the CXCR3 ligands are low to undetectable in NL, but they are markedly increased in inflammatory liver diseases (18, 36).

The CXCR3 ligands CXCL9, CXCL10, and CXCL11 are increased in chronic inflammatory liver disease as a consequence of secretion by hepatocytes, stromal cells, and endothelium. They can be readily detected on the glycocalyx of sinusoidal vessels (37–39), where they promote the transendothelial migration of effector T cells (18). We developed an in vitro flow-based adhesion assay in which primary cultures of HSECs are grown in microslides under physiological levels of shear stress to model the hepatic sinusoid (18). Treatment of HSECs with TNF-α and IFN-γ induces the expression of CXCL9, CXCL10, and CXCL11, as well as the adhesion molecules ICAM-1 and VCAM-1, thereby recapitulating the phenotype of chronically inflamed sinusoids in vivo (18). We used this assay in the current study to determine the role of CXCR3 on $LI-T_{regs.}$ We found that signaling through CXCR3 activated integrin-mediated arrest from flow and promoted the transendothelial migration of T_{regs} across inflamed hepatic sinusoidal endothelium. The fact that a similar degree of inhibition to both processes was seen when a blocking CXCR3 Ab or the G_{α} protein inhibitor PTx was used suggests that CXCR3 is the dominant chemokine receptor involved. All three CXCR3 ligands were involved in the in vitro flow assays, because blocking individual chemokines had a lesser effect than blocking the common receptor CXCR3. These findings are consistent with studies in murine models of inflammatory disease that report the requirement for CXCR3 expression to allow T_{regs} to be recruited to inflamed tissues in graft-versus-host disease (40) and to the brain in experimental autoimmune encephalomyelitis (41). Recently, CXCR3 has been implicated in the recruitment of T_{regs} into the murine liver in response to inflammation and IFN-γ production from NKT cells (42), and $Foxp3^+$ T_{regs} could upregulate Th1 specifying transcription factor T-bet, which, in turn, promote the expression of the chemokine receptor CXCR3 on T_{regs} in response to IFN-γ (43). Thus, IFN-inducible chemokines CXCL9 and CXCL10 expressed on inflamed hepatic sinusoidal endothelium promote the recruitment of CXCR3-expressing T_{regs} under shear stress as they do the recruitment of effector cells (18). A difference between the behavior of effector cells reported in our previous study and T_{regs} was the involvement of VCAM-1, but not ICAM-1, in the adhesion of T_{regs} to HSECs, whereas effector cells use ICAM-1 (18).

CCR4 is the other chemokine receptor that was strongly overexpressed on LIT_{regs}; it was coexpressed with CXCR3 in nearly 80% of T_{regs} from chronically inflamed livers. Liver-derived T_{regs} migrated to the CCR4 ligands CCL17 and CCL22 in vitro, demonstrating that the receptor is functional. CCR4 expression has been associated with T_{regs} and shown to control migration and immune suppression in the skin (44, 45) and in immunologically tolerant cardiac allografts (46). Until this report, CCR4 was not believed to play a role in the recruitment of T cells to the liver, and few effector cells in the liver express CCR4 (39). CCR4 is the receptor for two chemokines CCL17 and CCL22, both of which are secreted by DCs on maturation, and they recruit and retain T_{regs} in contact with DCs in lymph nodes (44, 47–51). The interaction between T_{regs} and DCs inhibits DC maturation and the expression of costimulatory molecules required for effector T cell activation (52–55). We were unable to detect either chemokine in normal human liver tissue by Western blotting of whole liver tissue or by immunohistochemistry. However, both chemokines were detected in inflamed liver tissue, and immunohistochemistry showed staining restricted to $CD11c^+$ DCs within inflammatory infiltrates in septal areas and lobules. To confirm that LIDCs secrete CCR4 ligands, we isolated myeloid DCs from liver tissue and showed that they expressed and secreted CCL17 and CCL22.

Confocal microscopy of liver tissue revealed that LIT_{regs} were closely associated with DCs and CD8 T cells in chronic hepatitis (Fig. 7), suggesting that they are ideally positioned to maintain intrahepatic immune suppression. We propose that localization to these infiltrates occurs in response to sequential chemokine signals. Local proinflammatory cytokines, including IFN-γ, lead to the secretion of CXCL9 and CXCL10 by sinusoidal and parenchyma cells; these chemokines are presented on the glycocalyx of sinusoidal endothelium where they recruit $CXCR3^{high}$ circulating T_{regs} into the liver. Subsequent migration within the inflamed liver is guided by CCR4, which allows tissue-infiltrating T_{regs} to respond to CCL17 and CCL22 secreted by activated intrahepatic DCs, thereby resulting in their accumulation within DC-rich inflammatory infiltrates in liver tissue.

This begs the question of why inflammation persists in the presence of so many T_{regs}. These cells are functional in vitro, but it is possible that their function is suppressed within the liver microenvironment in vivo. To investigate this possibility, we stained the intrahepatic T_{regs} in situ for phosphoSTAT5. STAT5 phosphorylation is a consequence of IL-2R activation and, thus, provides an indication of whether the intrahepatic T_{regs} are activated (56). We quantified the numbers of pSTAT5-positive cells in the liver and found that only 5–15% of the liver-infiltrating $FOXP3^+$ cells also expressed pSTAT5. Thus, it is possible that these cells are suppressed in situ, possibly by programmed death receptor-1–dependent mechanisms, as has been proposed for chronic HCV infection (57), allowing the effector arm to drive persistent inflammation.

Acknowledgments

We thank the staff at the Liver Transplant Unit, Queen Elizabeth Hospital, for their help with sample collection and the patients for donating blood and tissue. We also thank Nicholas Graham, Rebecca Adams, and Janine Youster for help with immunohistochemistry and Gill Muirhead for help with HSEC isolation and culture.

Disclosures

The authors have no financial conflicts of interest.

References

1. Sakaguchi, S., and F. Powrie. 2007. Emerging challenges in regulatory T cell function and biology. *Science* 317: 627–629.
2. Crispe, I. N., M. Giannandrea, I. Klein, B. John, B. Sampson, and S. Wuensch. 2006. Cellular and molecular mechanisms of liver tolerance. *Immunol. Rev.* 213: 101–118.
3. Rushbrook, S. M., M. Hoare, and G. J. Alexander. 2007. T-regulatory lymphocytes and chronic viral hepatitis. *Expert Opin. Biol. Ther.* 7: 1689–1703.
4. Unitt, E., S. M. Rushbrook, A. Marshall, S. Davies, P. Gibbs, L. S. Morris, N. Coleman, and G. J. Alexander. 2005. Compromised lymphocytes infiltrate hepatocellular carcinoma: the role of T-regulatory cells. *Hepatology* 41: 722–730.
5. Lan, R. Y., C. Cheng, Z. X. Lian, K. Tsuneyama, G. X. Yang, Y. Moritoki, Y. H. Chuang, T. Nakamura, S. Saito, S. Shimoda, et al. 2006. Liver-targeted and peripheral blood alterations of regulatory T cells in primary biliary cirrhosis. *Hepatology* 43: 729–737.
6. Longhi, M. S., M. J. Hussain, R. R. Mitry, S. K. Arora, G. Mieli-Vergani, D. Vergani, and Y. Ma. 2006. Functional study of CD4+CD25+ regulatory T cells in health and autoimmune hepatitis. *J. Immunol.* 176: 4484–4491.
7. Sakaguchi, S. 2004. Naturally arising CD4+ regulatory T cells for immunologic self-tolerance and negative control of immune responses. *Annu. Rev. Immunol.* 22: 531–562.

Downloaded from http://www.jimmunol.org/ by guest on February 24, 2022

8. Liu, W., A. L. Putnam, Z. Xu-Yu, G. L. Szot, M. R. Lee, S. Zhu, P. A. Gottlieb, P. Kapranov, T. R. Gingeras, B. Fazekas de St Groth, et al. 2006. CD127 expression inversely correlates with FoxP3 and suppressive function of human CD4+ T reg cells. *J. Exp. Med.* 203: 1701–1711.
9. Seddiki, N., B. Santner-Nanan, J. Martinson, J. Zaunders, S. Sasson, A. Landay, M. Solomon, W. Selby, S.I. Alexander, R. Nanan, et al. 2006. Expression of interleukin (IL)-2 and IL-7 receptors discriminates between human regulatory and activated T cells. *J. Exp. Med.* 203: 1693–1700.
10. Sakaguchi, S. 2005. Naturally arising Foxp3-expressing CD25+CD4+ regulatory T cells in immunological tolerance to self and non-self. *Nat. Immunol.* 6: 345–352.
11. Sakaguchi, S., N. Sakaguchi, M. Asano, M. Itoh, and M. Toda. 1995. Immunologic self-tolerance maintained by activated T cells expressing IL-2 receptor alpha-chains (CD25). Breakdown of a single mechanism of self-tolerance causes various autoimmune diseases. *J. Immunol.* 155: 1151–1164.
12. Tang, Q., and J. A. Bluestone. 2008. The Foxp3+ regulatory T cell: a jack of all trades, master of regulation. *Nat. Immunol.* 9: 239–244.
13. Ruprecht, C. R., M. Gattorno, F. Ferlito, A. Gregorio, A. Martini, A. Lanzavecchia, and F. Sallusto. 2005. Coexpression of CD25 and CD27 identifies FoxP3+ regulatory T cells in inflamed synovia. *J. Exp. Med.* 201: 1793–1803.
14. Cao, D., V. Malmström, C. Baecher-Allan, D. Hafler, L. Klareskog, and C. Trollmo. 2003. Isolation and functional characterization of regulatory CD25brightCD4+ T cells from the target organ of patients with rheumatoid arthritis. *Eur. J. Immunol.* 33: 215–223.
15. van Amelsfort, J. M., K. M. Jacobs, J. W. Bijlsma, F. P. Lafeber, and L. S. Taams. 2004. CD4(+)CD25(+) regulatory T cells in rheumatoid arthritis: differences in the presence, phenotype, and function between peripheral blood and synovial fluid. *Arthritis Rheum.* 50: 2775–2785.
16. Belkaid, Y. 2008. Role of Foxp3-positive regulatory T cells during infection. *Eur. J. Immunol.* 38: 918–921.
17. Strauss, L., C. Bergmann, M. Szczepanski, W. Gooding, J. T. Johnson, and T. L. Whiteside. 2007. A unique subset of CD4+CD25highFoxp3+ T cells secreting interleukin-10 and transforming growth factor-beta1 mediates suppression in the tumor microenvironment. *Clin. Cancer Res.* 13: 4345–4354.
18. Curbishley, S. M., B. Eksteen, R. P. Gladue, P. Lalor, and D. H. Adams. 2005. CXCR 3 activation promotes lymphocyte transendothelial migration across human hepatic endothelium under fluid flow. *Am. J. Pathol.* 167: 887–899.
19. Eksteen, B., A. Miles, S. M. Curbishley, C. Tselepis, A. J. Grant, L. S. Walker, and D. H. Adams. 2006. Epithelial inflammation is associated with CCL28 production and the recruitment of regulatory T cells expressing CCR10. *J. Immunol.* 177: 593–603.
20. Lai, W. K., S. M. Curbishley, S. Goddard, E. Alabraba, J. Shaw, J. Youster, J. McKeating, and D. H. Adams. 2007. Hepatitis C is associated with perturbation of intrahepatic myeloid and plasmacytoid dendritic cell function. *J. Hepatol.* 47: 338–347.
21. Goddard, S., J. Youster, E. Morgan, and D. H. Adams. 2004. Interleukin-10 secretion differentiates dendritic cells from human liver and skin. *Am. J. Pathol.* 164: 511–519.
22. Lalor, P. F., S. Edwards, G. McNab, M. Salmi, S. Jalkanen, and D. H. Adams. 2002. Vascular adhesion protein-1 mediates adhesion and transmigration of lymphocytes on human hepatic endothelial cells. *J. Immunol.* 169: 983–992.
23. Grant, A. J., S. Goddard, J. Ahmed-Choudhury, G. Reynolds, D. G. Jackson, M. Briskin, L. Wu, S. G. Hübscher, and D. H. Adams. 2002. Hepatic expression of secondary lymphoid chemokine (CCL21) promotes the development of portal-associated lymphoid tissue in chronic inflammatory liver disease. *Am. J. Pathol.* 160: 1445–1455.
24. Lai, W. K., P. J. Sun, J. Zhang, A. Jennings, P. F. Lalor, S. Hubscher, J. A. McKeating, and D. H. Adams. 2006. Expression of DC-SIGN and DC-SIGNR on human sinusoidal endothelium: a role for capturing hepatitis C virus particles. *Am. J. Pathol.* 169: 200–208.
25. Gramberg, T., E. Soilleux, T. Fisch, P. F. Lalor, H. Hofmann, S. Wheeldon, A. Cotterill, A. Wegele, T. Winkler, D. H. Adams, and S. Pohlmann. 2007. Interactions of LSECtin and DC-SIGN/DC-SIGNR with viral ligands: Differential pH dependence, internalization and virion binding. *Virology* 373: 189–201.
26. Penna, G., M. Vulcano, A. Roncari, F. Facchetti, S. Sozzani, and L. Adorini. 2002. Cutting edge: differential chemokine production by myeloid and plasmacytoid dendritic cells. *J. Immunol.* 169: 6673–6676.
27. Walker, L. S., A. Chodos, M. Eggena, H. Dooms, and A. K. Abbas. 2003. Antigen-dependent proliferation of CD4+ CD25+ regulatory T cells in vivo. *J. Exp. Med.* 198: 249–258.
28. Ni Choileain, N., M. MacConmara, Y. Zang, T. J. Murphy, J. A. Mannick, and J. A. Lederer. 2006. Enhanced regulatory T cell activity is an element of the host response to injury. *J. Immunol.* 176: 225–236.
29. Holmén, N., A. Lundgren, S. Lundin, A. M. Bergin, A. Rudin, H. Sjövall, and L. Ohman. 2006. Functional CD4+CD25high regulatory T cells are enriched in the colonic mucosa of patients with active ulcerative colitis and increase with disease activity. *Inflamm. Bowel Dis.* 12: 447–456.
30. O'Connor, R. A., K. H. Malpass, and S. M. Anderton. 2007. The inflamed central nervous system drives the activation and rapid proliferation of Foxp3+ regulatory T cells. *J. Immunol.* 179: 958–966.
31. Westendorf, A. M., M. Templin, R. Geffers, S. Deppenmeier, A. D. Gruber, M. Probst-Kepper, W. Hansen, R. S. Liblau, F. Gunzer, D. Bruder, and J. Buer. 2005. CD4+ T cell mediated intestinal immunity: chronic inflammation versus immune regulation. *Gut* 54: 60–69.
32. Longhi, M. S., Y. Ma, R. R. Mitry, D. P. Bogdanos, M. Heneghan, P. Cheeseman, G. Mieli-Vergani, and D. Vergani. 2005. Effect of CD4+ CD25+ regulatory T-cells on CD8 T-cell function in patients with autoimmune hepatitis. *J. Autoimmun.* 25: 63–71.
33. Rushbrook, S. M., S. M. Ward, E. Unitt, S. L. Vowler, M. Lucas, P. Klenerman, and G. J. Alexander. 2005. Regulatory T cells suppress in vitro proliferation of virus-specific CD8+ T cells during persistent hepatitis C virus infection. *J. Virol.* 79: 7852–7859.
34. Lim, H. W., J. Lee, P. Hillsamer, and C. H. Kim. 2008. Human Th17 cells share major trafficking receptors with both polarized effector T cells and FOXP3+ regulatory T cells. *J. Immunol.* 180: 122–129.
35. Lim, H. W., H. E. Broxmeyer, and C. H. Kim. 2006. Regulation of trafficking receptor expression in human forkhead box P3+ regulatory T cells. *J. Immunol.* 177: 840–851.
36. Harvey, C. E., J. J. Post, P. Palladinetti, A. J. Freeman, R. A. Ffrench, R. K. Kumar, G. Marinos, and A. R. Lloyd. 2003. Expression of the chemokine IP-10 (CXCL10) by hepatocytes in chronic hepatitis C virus infection correlates with histological severity and lobular inflammation. *J. Leukoc. Biol.* 74: 360–369.
37. Narumi, S., Y. Tominaga, M. Tamaru, S. Shimai, H. Okumura, K. Nishioji, Y. Itoh, and T. Okanoue. 1997. Expression of IFN-inducible protein-10 in chronic hepatitis. *J. Immunol.* 158: 5536–5544.
38. Tamaru, M., K. Nishioji, Y. Kobayashi, Y. Watanabe, Y. Itoh, T. Okanoue, M. Murai, K. Matsushima, and S. Narumi. 2000. Liver-infiltrating T lymphocytes are attracted selectively by IFN-inducible protein-10. *Cytokine* 12: 299–308.
39. Shields, P. L., C. M. Morland, M. Salmon, S. Qin, S. G. Hubscher, and D. H. Adams. 1999. Chemokine and chemokine receptor interactions provide a mechanism for selective T cell recruitment to specific liver compartments within hepatitis C-infected liver. *J. Immunol.* 163: 6236–6243.
40. Hasegawa, H., A. Inoue, M. Kohno, J. Lei, T. Miyazaki, O. Yoshie, M. Nose, and M. Yasukawa. 2008. Therapeutic effect of CXCR3-expressing regulatory T cells on liver, lung and intestinal damages in a murine acute GVHD model. *Gene Ther.* 15: 171–182.
41. Müller, M., S. L. Carter, M. J. Hofer, P. Manders, D. R. Getts, M. T. Getts, A. Dreykluft, B. Lu, C. Gerard, N. J. King, and I. L. Campbell. 2007. CXCR3 signaling reduces the severity of experimental autoimmune encephalomyelitis by controlling the parenchymal distribution of effector and regulatory T cells in the central nervous system. *J. Immunol.* 179: 2774–2786.
42. Santodomingo-Garzon, T., J. Han, T. Le, Y. Yang, and M. G. Swain. 2009. Natural killer T cells regulate the homing of chemokine CXC receptor 3-positive regulatory T cells to the liver in mice. *Hepatology* 49: 1267–1276.
43. Koch, M. A., G. Tucker-Heard, N. R. Perdue, J. R. Killebrew, K. B. Urdahl, and D. J. Campbell. 2009. The transcription factor T-bet controls regulatory T cell homeostasis and function during type 1 inflammation. *Nat. Immunol.* 10: 595–602.
44. Sather, B. D., P. Treuting, N. Perdue, M. Miazgowicz, J. D. Fontenot, A. Y. Rudensky, and D. J. Campbell. 2007. Altering the distribution of Foxp3(+) regulatory T cells results in tissue-specific inflammatory disease. *J. Exp. Med.* 204: 1335–1347.
45. Iellem, A., M. Mariani, R. Lang, H. Recalde, P. Panina-Bordignon, F. Sinigaglia, and D. D'Ambrosio. 2001. Unique chemotactic response profile and specific expression of chemokine receptors CCR4 and CCR8 by CD4(+)CD25(+) regulatory T cells. *J. Exp. Med.* 194: 847–853.
46. Lee, I., L. Wang, A. D. Wells, M. E. Dorf, E. Ozkaynak, and W. W. Hancock. 2005. Recruitment of Foxp3+ T regulatory cells mediating allograft tolerance depends on the CCR4 chemokine receptor. *J. Exp. Med.* 201: 1037–1044.
47. Katou, F., H. Ohtani, T. Nakayama, K. Ono, K. Matsushima, A. Saaristo, H. Nagura, O. Yoshie, and K. Motegi. 2001. Macrophage-derived chemokine (MDC/CCL22) and CCR4 are involved in the formation of T lymphocyte-dendritic cell clusters in human inflamed skin and secondary lymphoid tissue. *Am. J. Pathol.* 158: 1263–1270.
48. Curiel, T. J., G. Coukos, L. Zou, X. Alvarez, P. Cheng, P. Mottram, M. Evdemon-Hogan, J. R. Conejo-Garcia, L. Zhang, M. Burow, et al. 2004. Specific recruitment of regulatory T cells in ovarian carcinoma fosters immune privilege and predicts reduced survival. *Nat. Med.* 10: 942–949.
49. Cardoso, C. R., G. P. Garlet, A. P. Moreira, W. M. Júnior, M. A. Rossi, and J. S. Silva. 2008. Characterization of CD4+CD25+ natural regulatory T cells in the inflammatory infiltrate of human chronic periodontitis. *J. Leukoc. Biol.* 84: 311–318.
50. Tang, H. L., and J. G. Cyster. 1999. Chemokine up-regulation and activated T cell attraction by maturing dendritic cells. *Science* 284: 819–822.
51. Vulcano, M., C. Albanesi, A. Stoppacciaro, R. Bagnati, G. D'Amico, S. Struyf, P. Transidico, R. Bonecchi, A. Del Prete, P. Allavena, et al. 2001. Dendritic cells as a major source of macrophage-derived chemokine/CCL22 in vitro and in vivo. *Eur. J. Immunol.* 31: 812–822.
52. Sansom, D. M., and L. S. Walker. 2006. The role of CD28 and cytotoxic T-lymphocyte antigen-4 (CTLA-4) in regulatory T-cell biology. *Immunol. Rev.* 212: 131–148.
53. Wing, K., Y. Onishi, P. Prieto-Martin, T. Yamaguchi, M. Miyara, Z. Fehervari, T. Nomura, and S. Sakaguchi. 2008. CTLA-4 control over Foxp3+ regulatory T cell function. *Science* 322: 271–275.
54. Houot, R., I. Perrot, E. Garcia, I. Durand, and S. Lebecque. 2006. Human CD4 +CD25high regulatory T cells modulate myeloid but not plasmacytoid dendritic cells activation. *J. Immunol.* 176: 5293–5298.
55. Bayry, J., F. Triebel, S. V. Kaveri, and D. F. Tough. 2007. Human dendritic cells acquire a semimature phenotype and lymph node homing potential through interaction with CD4+CD25+ regulatory T cells. *J. Immunol.* 178: 4184–4193.
56. O'Gorman, W. E., H. Dooms, S. H. Thorne, W. F. Kuswanto, E. F. Simonds, P. O. Krutzik, G. P. Nolan, and A. K. Abbas. 2009. The initial phase of an immune response functions to activate regulatory T cells. *J. Immunol.* 183: 332–339.
57. Franceschini, D., M. Paroli, V. Francavilla, M. Videtta, S. Morrone, G. Labbadia, A. Cerino, M. U. Mondelli, and V. Barnaba. 2009. PD-L1 negatively regulates CD4+CD25+Foxp3+ Tregs by limiting STAT-5 phosphorylation in patients chronically infected with HCV. *J. Clin. Invest.* 119: 551–564.

Downloaded from http://www.jimmunol.org/ by guest on February 24, 2022